CHAPTER 3

SECTION (A)

Grafted polymeric organogel as an effective medium for removal of cationic dyes and organic pollutants from contaminated water

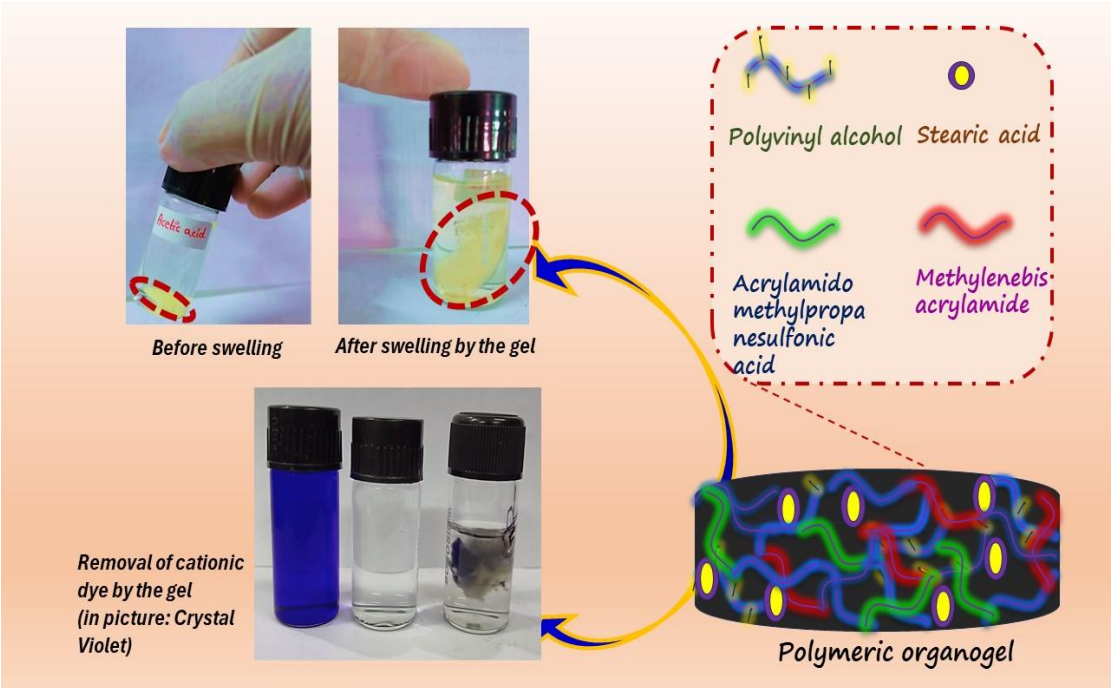

This chapter describes the preparation procedure of the organogel followed by its application in dye removal and absorption of organic solvent.

This part of the thesis is published in

Baruah, K., Dutta, R., Doley, S., and Dolui, S.K. Grafted polymeric organogel using low molecular weight gelator as an effective medium for expulsion and purification of cationic dyes and organic pollutants from contaminated surface water. ***European Polymer Journal***, 195, 112213, 2023

3.1 INTRODUCTION

With the advancement of technology and the growth of industries, contamination of water resources has become a significant issue in nearby areas. This is mainly due to the release of pollutants and toxic chemicals into water bodies as residual waste. The untreated wastewater, which contains a high concentration of organic and inorganic materials, poses a threat to the entire ecosystem [1,2]. The textile and paper industry, in particular, heavily relies on dyes to impart colors, resulting in more than 80% of effluents being discharged into water bodies [4]. These dyes are highly soluble in water and difficult to separate, leading to severe pollution of the environment and the emergence of carcinogenic issues [5,6]. The complex structure of the dyes, with multiple aromatic rings, makes them resistant to biodegradation. In addition to dyes, industrial waste also includes the release of organic solvents [9–11], hazardous heavy metals [12,13], and hydrocarbons [14,15], which pose a challenge for the removal of these toxic pollutants [16]. These pollutants persist in the environment for a long time, affecting the aquatic and terrestrial ecosystems [17,18].

Various methods have been proposed for the removal of these pollutants, including membrane filtration, coagulation and flocculation, ion exchange, advanced oxidation processes, electrochemical oxidation, and microbial technologies [19–23]. However, each method has its limitations. For example, membrane filtration requires high differential pressure and costly repairs. Coagulation, both chemical and electrochemical, requires the addition of chemicals, resulting in sludge formation that poses disposal concerns. The ion exchange method has limitations in terms of reducibility and the regenerated fluid containing harmful ions.

Among the aforementioned processes, adsorption and photocatalytic degradation have shown promise in the removal of toxic dyes [24-27]. However, photocatalytic processes often leave behind scavenging materials in the treated water, which can pose threats to aquatic species and serious health issues for humans [28,29]. To address these challenges and provide effective treatment of the generated waste products, adsorbent-based systems offer a safer and more environmentally friendly approach. These systems are widely used due to their selectivity, high efficiency, adaptability, ease of production, and cost-effectiveness [30–33]. In this study, an organogel has been employed as an adsorbent for the selective absorption of organic solvents [34] and the adsorption of

discharged dyes (specifically cationic dyes) from contaminated water sources resulting from industrial waste.

Polymers in the form of composites [35–38], activated carbon [39,40], and polymer hybrids [41,42] are widely used for the removal of dye molecules. A soft form of polymer, hydrogel has also been used for removal purpose however cases with organogel has been rarely reported [43,44]. A solvent-based gel, when dipped in water will infuse less amount of water and bind with the dye molecules through electrostatic attraction and surface adsorption thereby will adsorb more of the toxic pollutants mixed with water rather than hydrogel which might infuse a heavy amount of water, chances of leaving behind toxic molecules. Hence an organogel has been preferred for use in wastewater treatment. With this content, a modification of our previous work, the synthesis of organogel used for the removal of organic solvents from contaminated water sources [45] has further been modified to adsorb dye molecules for the remedial treatment of water resources.

The current study focuses on the application of adsorbents as promising materials for the removal of effluents from untreated wastes. This is achieved by modifying previous research and incorporating acrylamide-methylpropane sulfonic acid as a co-monomer with methylene-bis-acrylamide as a crosslinker. This modification allows for selective adsorption of cationic species due to the presence of the negatively charged sulfonic group. Experimental results show that in addition to effectively absorbing solvents, the organogel is also able to selectively adsorb cationic dyes (such as crystal violet, gentian violet, and ethyl purple) from aqueous solutions. This is attributed to the interaction between the sulfonic group and positively charged species, making the organogel an effective sorbent for water purification. However, the primary focus of this study is on the absorption of solvents as well as the adsorption of cationic dyes from contaminated water sources. In addition to examining kinetic equations, isothermic and diffusion models were also studied to elucidate the mechanism of the adsorption process.

This study aims to employ LMWGs for the purification of contaminated sources. Specifically, octadecanoic acid (also known as stearic acid) is used as LMWG. It is further grafted and modified to effectively remove contaminants from water bodies, such as toxic dyes or harmful organic pollutants. The use of simple and cost-effective materials, namely fatty acid and polyvinyl alcohol (PVA) grafted with AMPS-based

organogel, is advantageous for sustainable development. Furthermore, the biodegradable and recyclable nature of the materials adds to their environmental benefits.

3.2 EXPERIMENTAL SECTION

3.2.1 Materials

Acrylamidomethylpropanesulfonic acid (AMPS), Methylene bisacrylamide (MBA), and Crystal violet were purchased from Sigma Aldrich. Rankem chemicals provided Methyl violet (Gentian violet B), chloroform, and tetrahydrofuran. Dimethyl sulfoxide (DMSO), methanol, benzene, ethylene glycol, acetic acid, dichloromethane, toluene, and carbon tetrachloride were procured from Merck. Ammonium persulfate (APS) and dimethylformamide (DMF) were brought from SRL while stearic acid (SA) from Loba Chemie Pvt. Ltd. Polyvinyl Alcohol (PVA) (MW:14000) was obtained from Otto (Chemika-biochemika reagents) while p-toluenesulfonic acid (98%) from BDH laboratory supplies and Ethyl violet (ethyl purple) from Himedia. Absolute alcohol was purchased from Helix India. All the chemicals received were of analytical grade and were used as received.

3.2.2 Preparation of the organogel:

The organogel was prepared by a reaction between PVA, Stearic acid, AMPS along with MBA and oxidant APS. Herein, 0.214mmol of PVA was stirred with 15mL of DMSO in a round bottom flask equipped with a thermometer placed over a magnetic stirrer at a temperature of about 80-85 ºC. *p*-TSA was added to the RB along with stearic acid (Table 3.1) of different concentrations and the mixture was allowed for continuous stirring for 1 hour. To the dissolved mixture, subsequently, AMPS (0.34 mM) in correspond to PVA was added. It was proceeded by further addition of a solution of initiator APS(2.8 µM) and cross-linker MBA (0.202 mM) while the reaction was stirred for another 6 hours until the formation of a ‘gel-like substance appears. The product was washed several times with sodium bicarbonate solution followed by ethanol for neutralization and removal of unreacted components. The obtained gel was dried in a vacuum oven for 72 hours at 40ºC.

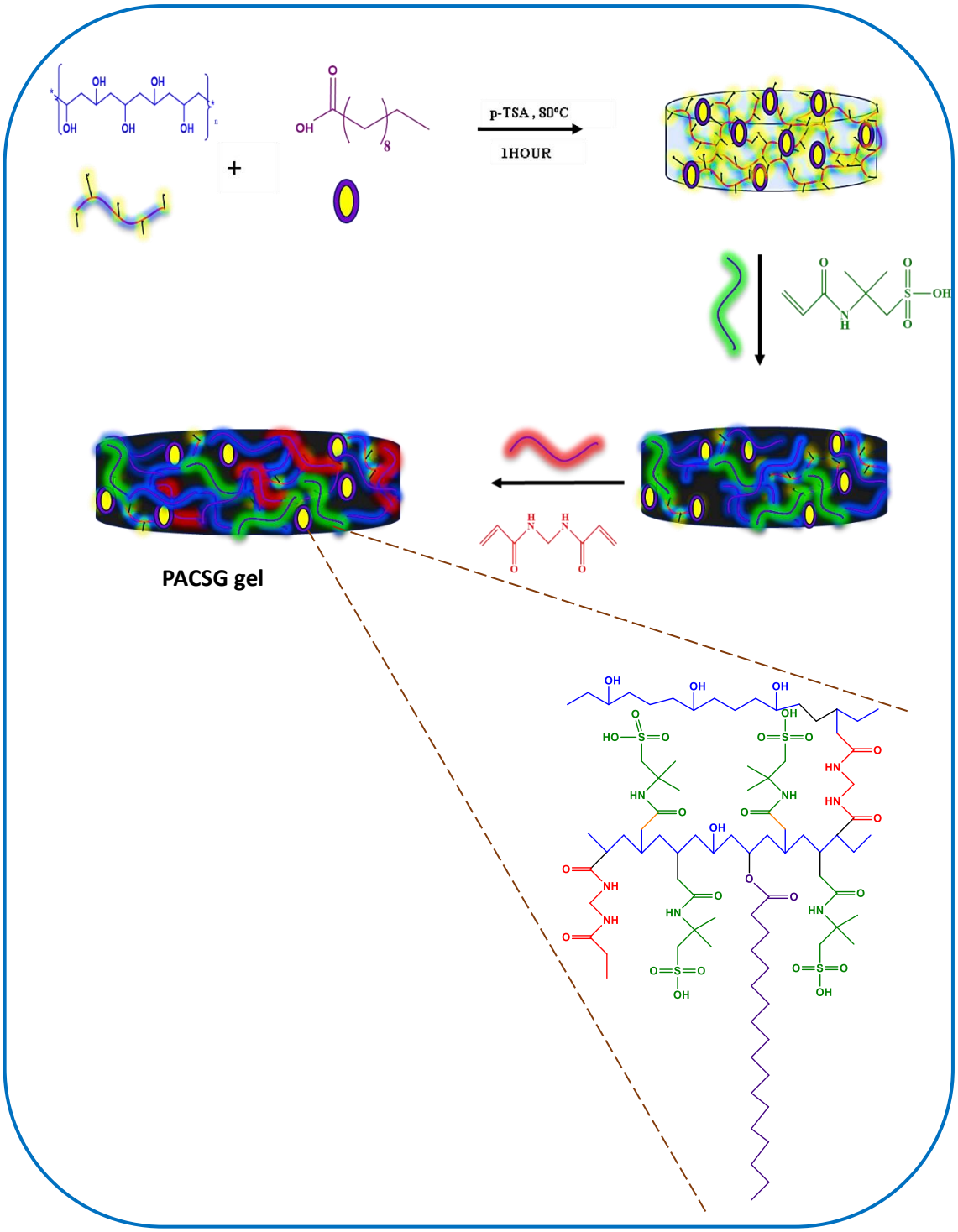

Scheme 3.1 Schematic illustration of the network of cross-linked organogel PACSG formed

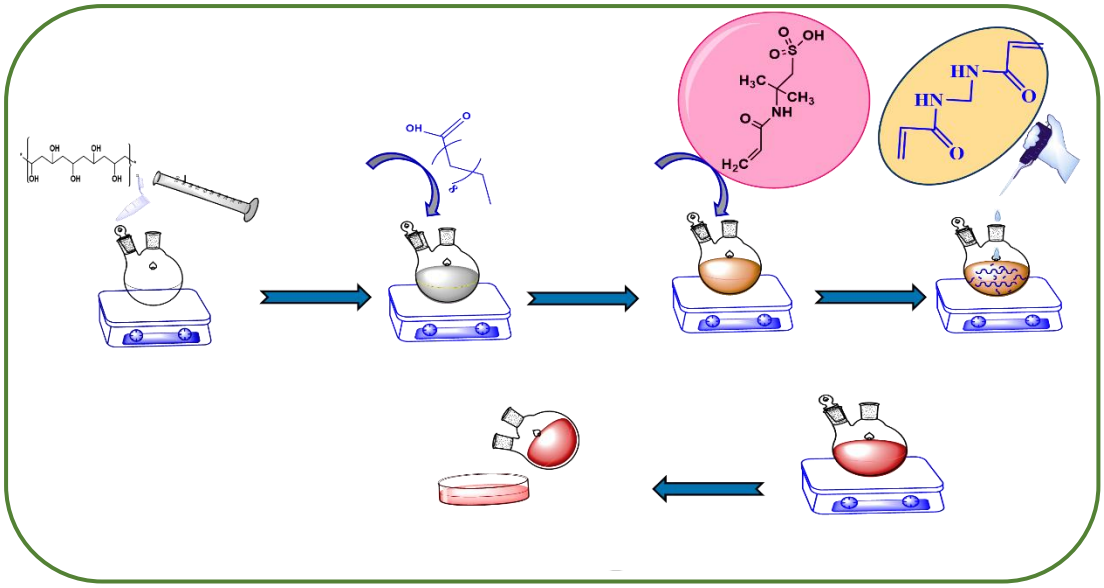

Figure 3.1 Step wise reactions involved during formation of PACSG organogel

Table 3.1 Composition chart of the prepared PACSG gels

SAMPLE	PVA (mM)	AMPS (mM)	Stearic Acid (mM)	Nature of material	WCA (⁰)
PACSG-26	0.214	0.34	26.01	Gel	85.2
PACSG-39	0.214	0.34	39.02	Gel	103.2
PACSG-52	0.214	0.34	52.03	Gel	104.6

3.2.3 Characterization:

The instruments used for characterization including WCA, FT-IR, SEM, TGA, DSC, XRD and rheology tests as mentioned in section 2.2.3 of Chapter 2. Quantitative determination of the analytes was performed using UV-Vis spectrophotometer SHIMADZU UV-2600I.

3.3 RESULTS AND DISCUSSION

3.3.1 Preparation and Characterization of the organogel

PVA reacts with stearic acid through an esterification reaction. With the addition of AMPS and MBA, it forms a cross-linked structure. The nature of part of the gel is hydrophobic due to stearic acid however, the other part is hydrophilic with the addition of ionizable AMPS, along with MBA as a crosslinker. This cross-linked inter-penetrating network of the gel gets enlarged, opening pores inside the gel matrix and making space available for entrapping solvents. The interweaving of the sulphonic groups also creates hydrophilic centers inside the matrix of the gel along with anionic

sites capable of adsorbing cationic species resulting in the increase of swelling as well as adsorption ability. The gel thus consists of balanced nature of both hydrophobic as well as hydrophilic character. The presence of the sulphonic group greatly enhances the adsorption ability of the adsorbent. It was also observed that while increasing the stearic acid content in the organogel, the water contact angle (WCA) seemed to increase drastically from a hydrophilic PVA chain to a hydrophobic state of gel formation (Images can be viewed below).

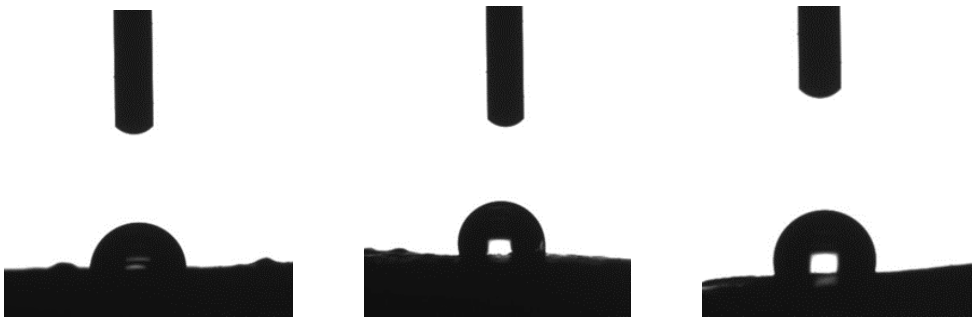

PACSG 26	PACSG 39	PACSG 52
WCA = 85.2º	WCA = 103.2º	WCA = 104.6º
Hydrophilic	Hydrophobic	Hydrophobic

Figure 3.2 Hydrophobicity data obtained from water contact angle analysis for the prepared organogels

3.3.1.1 FT-IR analysis

The synthesis of the prepared organogel was verified by FT-IR spectra determination as shown in Figure 3.3. The characteristics peak assigned at 1639.11cm^{-1} is due to the C=O vibrational stretching of MBA and AMPS grafting onto the PVA backbone while 1502.84cm^{-1} refers to the N–H bending of the amine. The absorption peak at 1242.63cm^{-1} refers to the C–N group while frequencies at 1180.65cm^{-1} and 1041.73cm^{-1} are due to the asymmetric and symmetric group of the SO_3H group. 1382.25cm^{-1} and 1026.84cm^{-1} refers to the S=O and S–O stretching of the sulfonic group [47]. Peaks at 1742.89cm^{-1} and 1119.42cm^{-1} contributed to the C=O stretching and C–O stretching of the formed ester group. The broad peaks at 3436.85cm^{-1} are due to the overlapping of the O–H and N–H groups with strong hydrogen bonding. Obtained peaks at 2925.89cm^{-1}, 2854.23cm^{-1}, and 1457.02cm^{-1} prefers the stretching of CH_3 and CH_2 groups along with bending vibration of C–H thus confirming the structural formation. Fingerprint region peaks at 721.45cm^{-1} and 625.88cm^{-1} are attributed to the cis and trans bending of C–H.

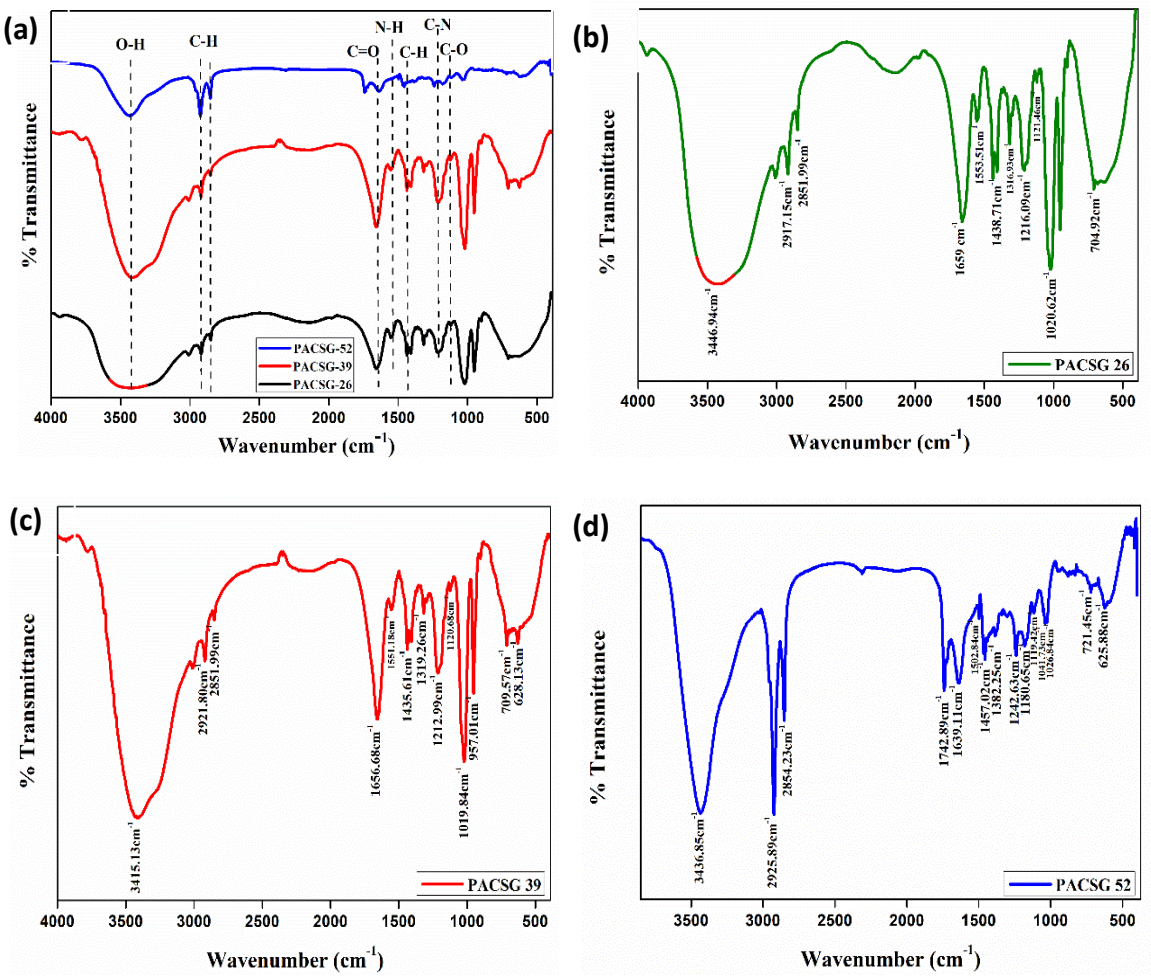

Figure 3.3 FT-IR spectra of (a) the prepared PACSGs, (b) PACSG-26, (c) PACSG-39, (d) PACSG-52

3.3.1.2 Morphological analysis

Corresponding images for the morphological structure were investigated using SEM. As shown in Figure 3.4a, the pristine PVA indicated an unvarying structural feature while that of AMPS (Figure 3.4b) consisted of some bristle-like arrangement which however on reaction with MBA transformed into a rough framework with further deposition of stearic acid. Grafting of AMPS led to an accumulation of sulfonic groups on the surface which was not observed in our previous work. However, the opening of porous surface and cross-linking sites were observed on the insertion of MBA as a cross-linker conferring an insight into the morphological study of organogel. EDX spectra of the organogel with elemental percentage are described in Figure 3.5.

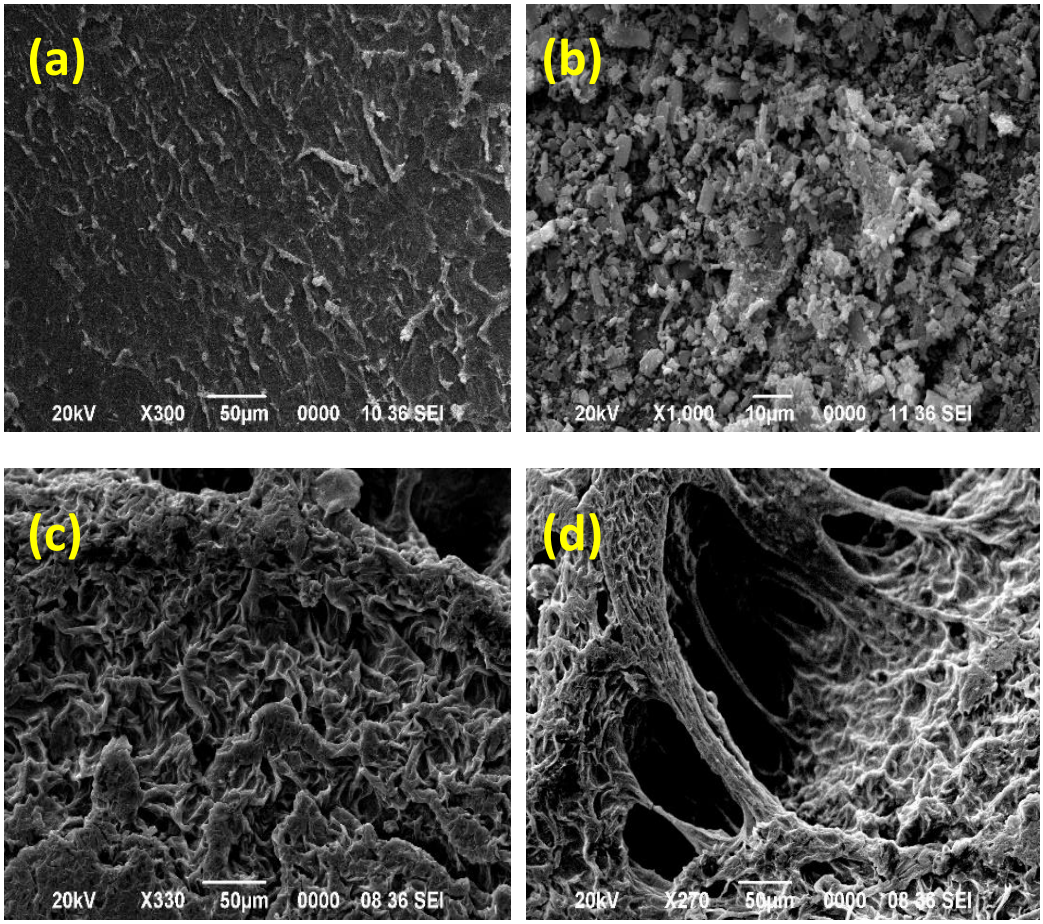

Figure 3.4 SEM micrographs of (a) PVA, (b) AMPS, (c) PACSG, (d) cross-linked pores of PACSG

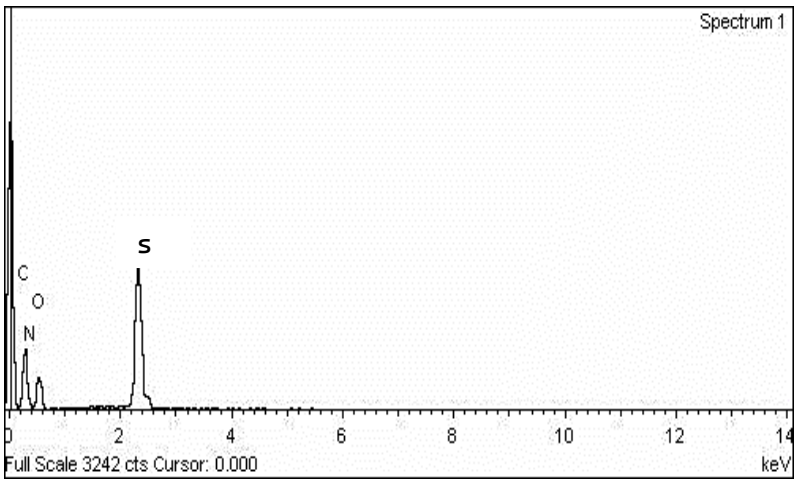

Element	Weight %
C K	40.89
N K	9.10
O K	34.20
S K	15.81
Totals	100.00

Figure 3.5 EDX spectra and elemental determination of the organogel PACSG-52

3.3.1.3 Thermal analysis

The thermal stability was characterized using TGA (Figure 3.6a). Pristine PVA observed degradation around 320ºC which can be perceived from a PVA-based organogel [45] however PVA-SA was seen around 220 ºC. Although on further addition

of AMPS to the PVA chain, the degradation rate increased due to lower blending stability between PVA and bulky AMPS group. However, the first degradation was seen around 167 ºC which further decreased down to 273 ºC due to evaporation or decomposition of SO_2 and SO_3 groups [49]. The next degradation around 328 ºC was due to the breaking of the PVA chain.

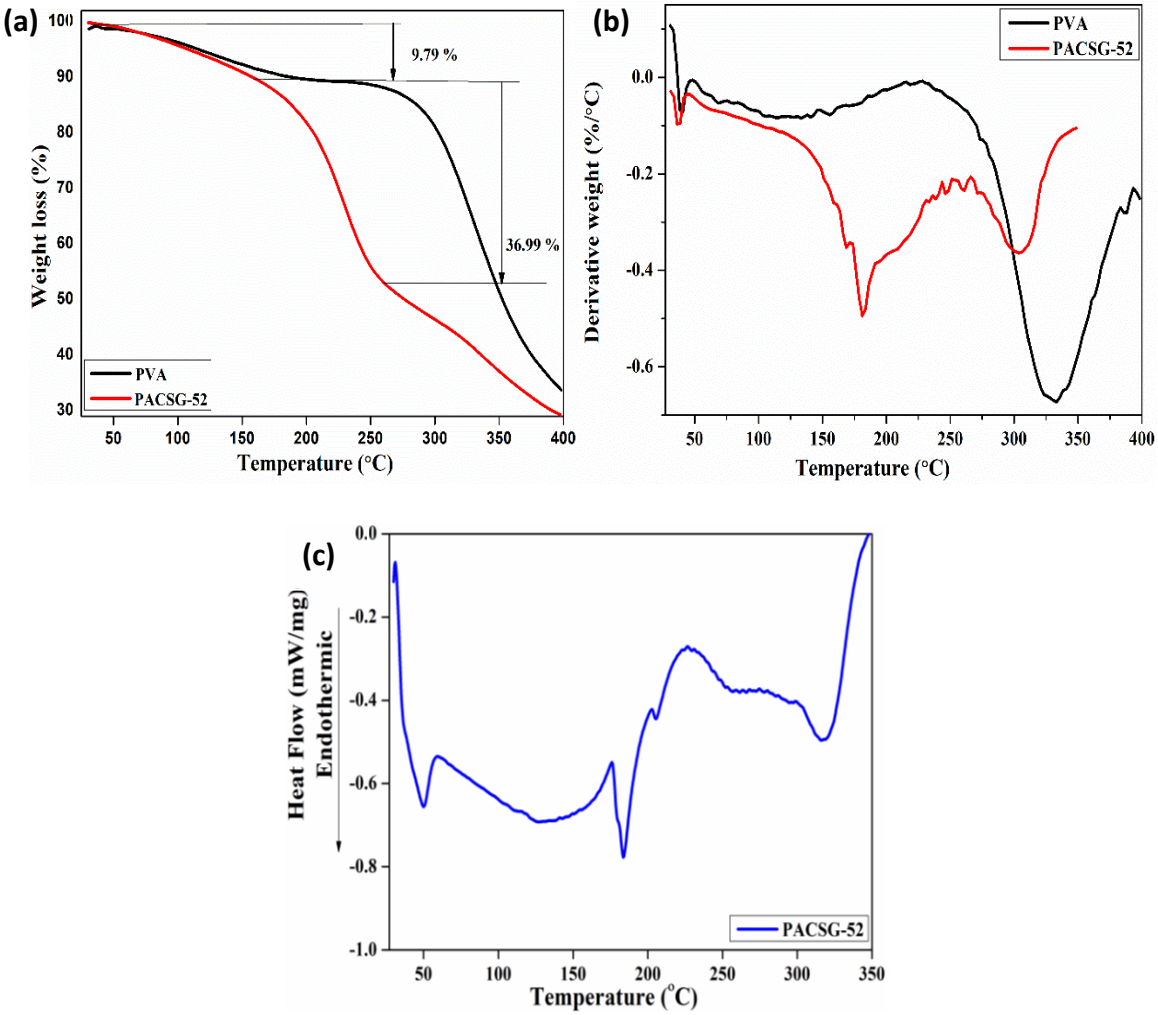

Figure 3.6 (a)TGA thermogram, (b) DTG curve, (c) DSC plot of PACSG-52

From, the DTG curve (Figure 3.6b), it can be perceived that dual-step weight loss was attained. The first melting temperature was observed around 182 ºC which however observed an early degradation due to the decomposition of functional groups present. A slight decrease around 254 ºC was due to the breakage of cross-linking bonds. Nonetheless, the second weight loss of around 304 ºC was due to the splitting of PVA bonds.

Figure 3.6c demonstrates the DSC curves which indicated the T_{max} temperature at 184 ºC due to the onset of thermal degradation of PVA-AMPS while a lower drop around 127ºC was observed due to loss of water molecules. Deterioration of cross-

linking bonds was observed around 258 ºC which further correlates with TG and DTG curves.

3.3.1.4 XRD & Rheological analysis

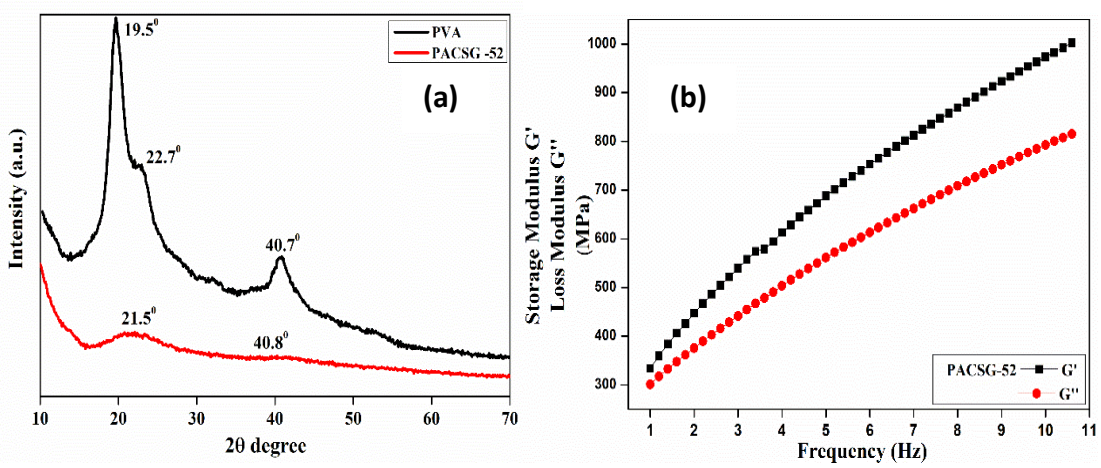

Figure 3.7 (a) XRD spectra of PACSG-52 gel, (b) data of storage and loss modulus from frequency sweep of PACSG-52

XRD data (Figure 3.7a) of PVA shows the peak of 2θ degrees at 19.5º, 22.7º, and 40.7º with planes corresponding to (101), (200), and (102) [48]. On further insertion of AMPS, the crystalline nature of PVA diminished to a greater extent. The peaks associated with PVA can be attained from the modified composite based on PVA and magnetite prepared by Modrogan et al [48]. The broad peak with the plane (102) observed around 40.7 ºC in PVA-SA interaction was seen to diminish indicating an extreme amorphous nature of the gel. Data obtained from the frequency sweep experiment in Figure 3.7b, denotes the elastic behaviour (G′>G″) of the gel as the deforming ability was found to be increase in comparison to flow behaviour.

3.3.2 Swelling Analysis

The structure demonstrated in Figure (3.4) obtained from SEM images alluded to the entrapment of organic solvents inside the gel matrix. The uptake of different organic solvents with varying polarities such as acetic acid, carbon tetrachloride, toluene, ethylene glycol, ethanol, dimethylformamide, benzene, tetrahydrofuran, diethylene glycol, chlorobenzene, dimethylaniline, chloroform along with methanol was investigated by the prepared cross-linked gels PACSG (26,39,52) as shown in Figure 3.8. However, among the three, PACSG-52 displayed excellent swelling behavior of organic solvents. The results of which are displayed in Figure 3.9.

The gels can absorb both polar and non-polar solvents as the gel possess dual functional groups of being hydrophobic for the stearic group and hydrophilic for the sulfonated group. It was ascertained from the swelling studies that the organogel swelled maximal in acetic acid for all the sets.

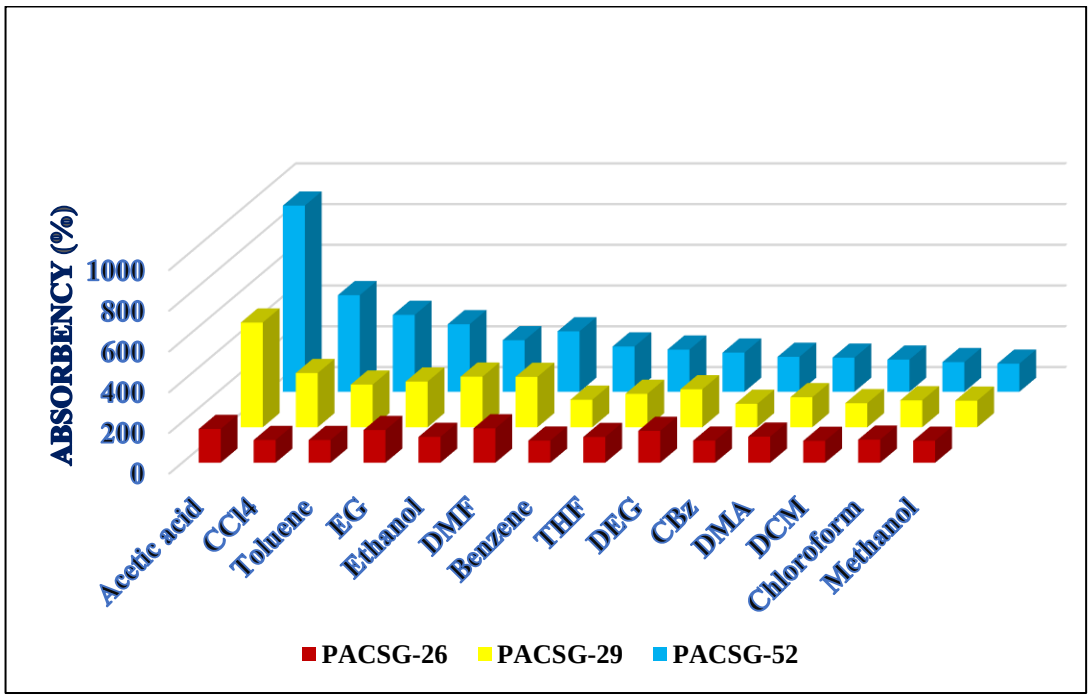

Figure 3.8 Swelling analysis of the prepared PACSG-26,39,52 gels in different solvents

The highest absorbance was exhibited by set PACSG-52 with swelling of more than 900% for acetic acid. The observed phenomenon can be attributed to intermolecular hydrogen bonding between solvent molecules and the gelator, resulting in an enhanced uptake of solvents. Carbon tetrachloride, toluene, ethylene glycol, and dimethyl formamide exhibited swelling in the range of 500-300% whereas ethanol, benzene, tetrahydrofuran, diethylene glycol, chlorobenzene, dimethyl aniline, dichloromethane, chloroform, and methanol lies in the range 250-150%. The absorption values of solvents can be correlated with both the dielectric constant values as well as the polarity of the organic solvents as they can simultaneously absorb both polar as well as non-polar solvents. Lower dielectric values denote a lesser ability to stabilize the charges present resulting in the probability of dipole-dipole interaction between sorbent and acetic acid being observed to be higher than those of dipole-induced dipole interaction in non-polar solvents or the involvement of hydrogen bonding in polar protic solvents.

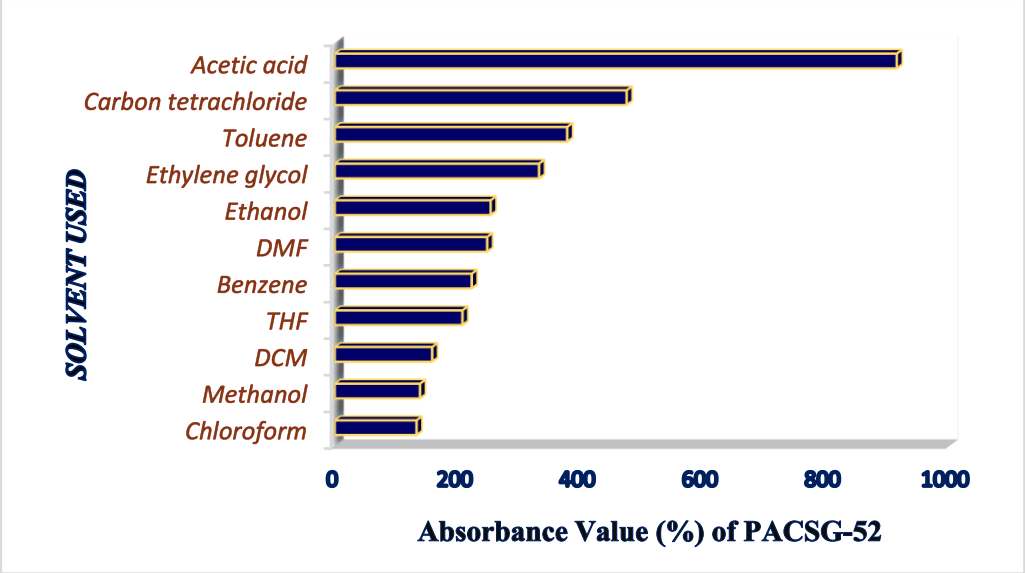

Figure 3.9 Swelling behavior observed by PACSG-52 gel

3.3.2.1 Swelling Kinetics of solvent

The solvent absorption efficiency of organic solvents onto the sorbent was investigated by a kinetic study using equations (iii) and (v) from section 2.2.5 of Chapter 2. The swelling kinetics of the prepared set of gels were evaluated considering the solvent of high absorbance, Acetic acid. Figure 3.10 displays the linear fitted curves for pseudo-first order and pseudo-second order kinetics models. However, the curves obtained a suitable linear correlation regression value(R^2) from a pseudo-second-order kinetics graph (Figure 3.11b) in which the plot of t/Q against time confirmed the absorption of solvents to the sorbent following the second-order model. The correlation coefficient value of 0.98 suggested a similar concordance between actual and experimented values. Values of k_1, and k_2 along with Q_{max} and R^2 for both models can be procured from Table 3.2.

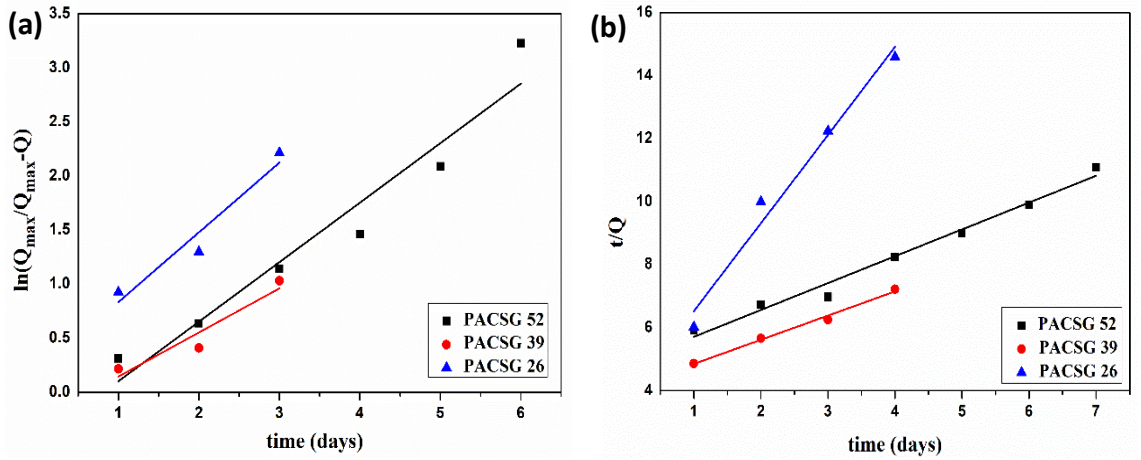

Figure 3.10 Plot for (a)first order, (b)second order kinetics graph of PACSG-52 gel

Table 3.2 Parameters for first and second-order kinetic models

SAMPLE	pseudo-first-order kinetics model			pseudo-second-order kinetics model		
	$k_1(min^{-1})$	$Q_{max}(gg^{-1})$	R^2	$k_2(gg^{-1}min^{-1})$	$Q_{max}(gg^{-1})$	R^2
PACSG-26	4.479×10^{-4}	0.275	**0.88**	0.238×10^{-4}	2.796	**0.96**
PACSG-39	2.833×10^{-4}	0.823	**0.83**	2.89×10^{-4}	0.767	**0.98**
PACSG-52	3.819×10^{-4}	0.631	**0.92**	1.96×10^{-4}	0.852	**0.97**

3.3.2.2 Reusability of solvent

The reusability (absorption and desorption) of the sorbent for solvent was examined using chloroform as the solvent. A certain weight of the sorbent was immersed in the solvent for a period of 24 hours. After the completion of 24 hours, the swollen gel was allowed to release the solvent from the gel-matrix structure by letting it dry at room temperature. The process was continued for 10 repetitive cycles to study the absorbance efficiency. Figure 3.11a depicts the percentage of solvent absorbance with each cycle. The study of recyclability was reported under the absorption and desorption cycle (Figure 3.11b) and with each cycle, the absorbed solvent was completely able to desorb and thus regain back its original shape to absorb solvent. Thus, it can be concluded that the sorbent can be re-generated multiple times after the desorption of solvent absorbed by the sorbent which suggests the use of sorbent for further removal of solvent from polluted water sources.

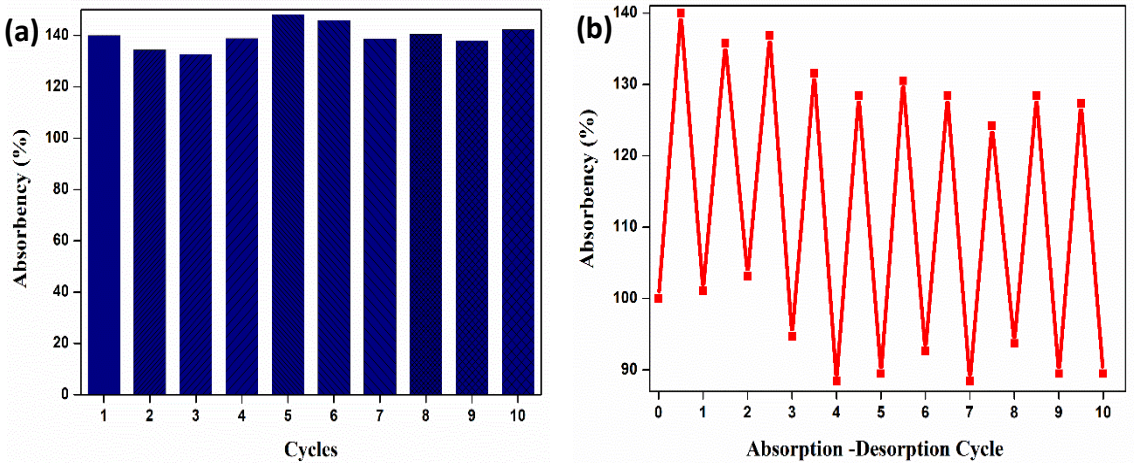

Figure 3.11 Recyclability data: (a) Solvent absorbance percentage with each cycle, (b) Absorption-desorption cycle of the solvent

3.3.3 Dye Adsorption

Of the prepared organogels, the one with excessive swelling PACSG-52 was chosen as sorbent for adsorption of cationic dyes CV, EV, and MV. The adsorption of dyes concerning time was recorded via UV-Vis spectroscopy, where it was seen that after the insertion of sorbent into the dye solution, the concentration of dyes gradually decreases with an increase in time.

The dye adsorption capability was investigated by dissolving water-soluble dyes (Crystal violet, Ethyl violet, and Methyl violet) prepared in distilled water with an initial concentration of 3×10^{-5} M for each of the respective dye solutions. After the preparation of dye solutions, an adsorbent of weight 0.2 gm was immersed in 200mL of previously prepared stock solution of dyes. At a certain time interval, the dye was extracted from the sample solution and the decrease in the concentration of dyes was measured along with the measurement of absorbance maxima (λ_{max}) in the UV-Vis spectrophotometer. The adsorption capacity of dyes and their removal efficiency by the adsorbent were evaluated according to the equation:

$$q_e = C_{o-}C_e/W \times V \quad \textbf{(i)}$$

$$\%\, Removal = C_o - C_e/C_o \times 100 \quad \textbf{(ii)}$$

where, qe (mg/g) is the amount of dye absorbed at equilibrium by the adsorbent

Co(mg/L) and Ce(mg/L) is the initial and equilibrium concentration

V(L) is the volume of the solution used

W(g) is the mass of the adsorbent used.

From the UV plot (Figure 3.12), it can be perceived that the sorbent/organogel can adsorb EV dye and the change of color can be noticed within 60 minutes while that of CV in 150 minutes and MV in 300 minutes respectively. The removal efficiency includes 99.35% for EV dye, 95.06% for CV, and 92.71% for MV dye (Table 3.3). The quicker removal can be explained due to the involvement of the easily ionizable sulfonic group in abundance as active sites reacting with imine groups present in the dyes interacting electrostatically along with the involvement of hydrogen bonding.

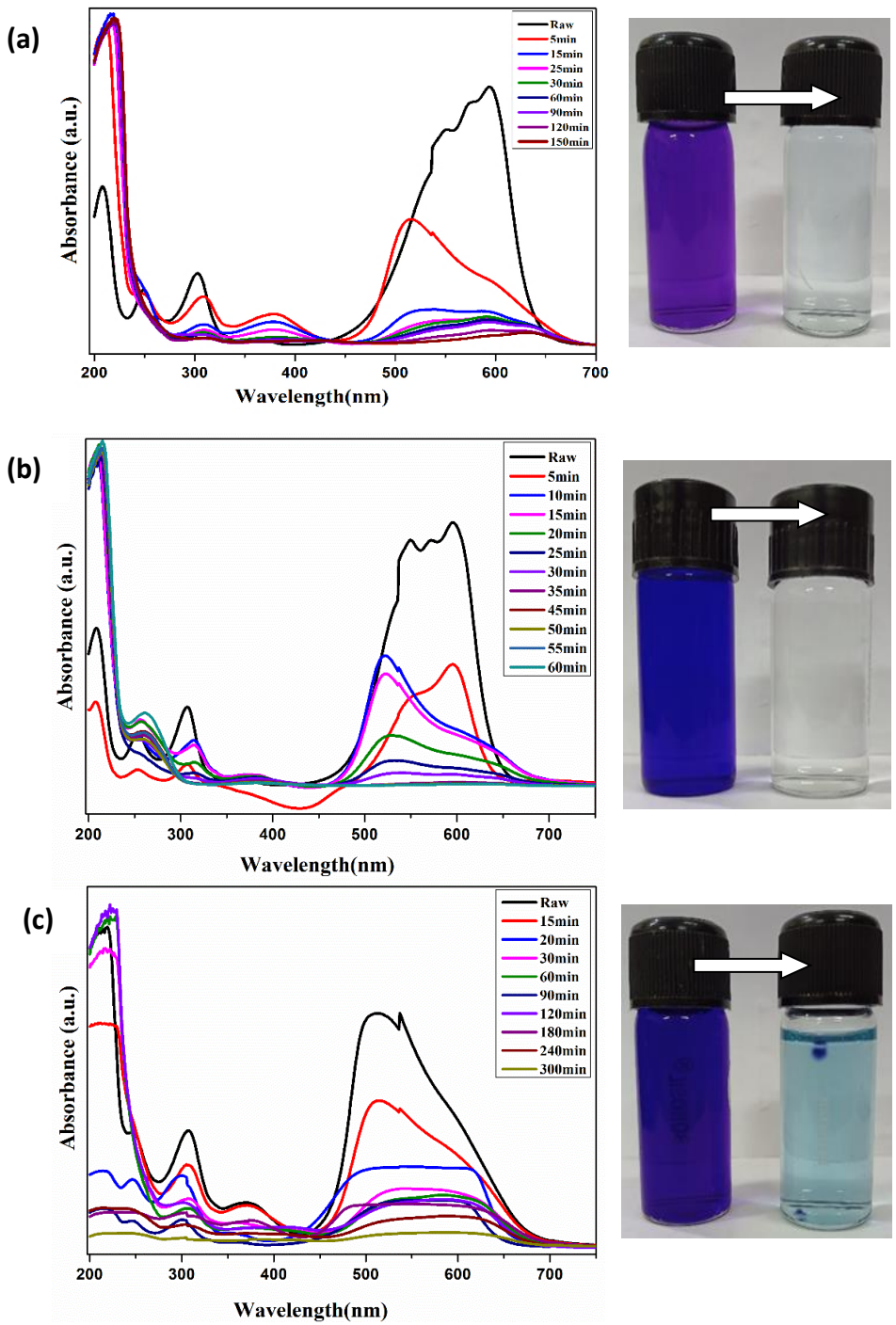

Figure 3.12 UV-Vis spectra of the adsorbent with time along with digital images of dyes before and after removal by the adsorbent for (a) CV dye, (b) EV dye, and (c) MV dye

Table 3.3 Removal efficiency of dyes with concentration before and after removal

Adsorbate	Concentration before adsorption (M)	Concentration after adsorption (M)	Removal Efficiency (%)
Crystal Violet	3.24×10^{-5}	0.16×10^{-5}	**95.06**
Ethyl Violet	3.10×10^{-5}	0.02×10^{-5}	**99.35**
Methyl Violet	3.32×10^{-5}	0.24×10^{-5}	**92.71**

It can be concluded from Table 3.3 that the uptake of Ethyl violet was the maximum out of the three selected cationic dyes. The presence of negatively charged sulfonic groups present in the gel-matrix acts as an active site for interaction with cationic polluted dyes speeding up the adsorption rate.

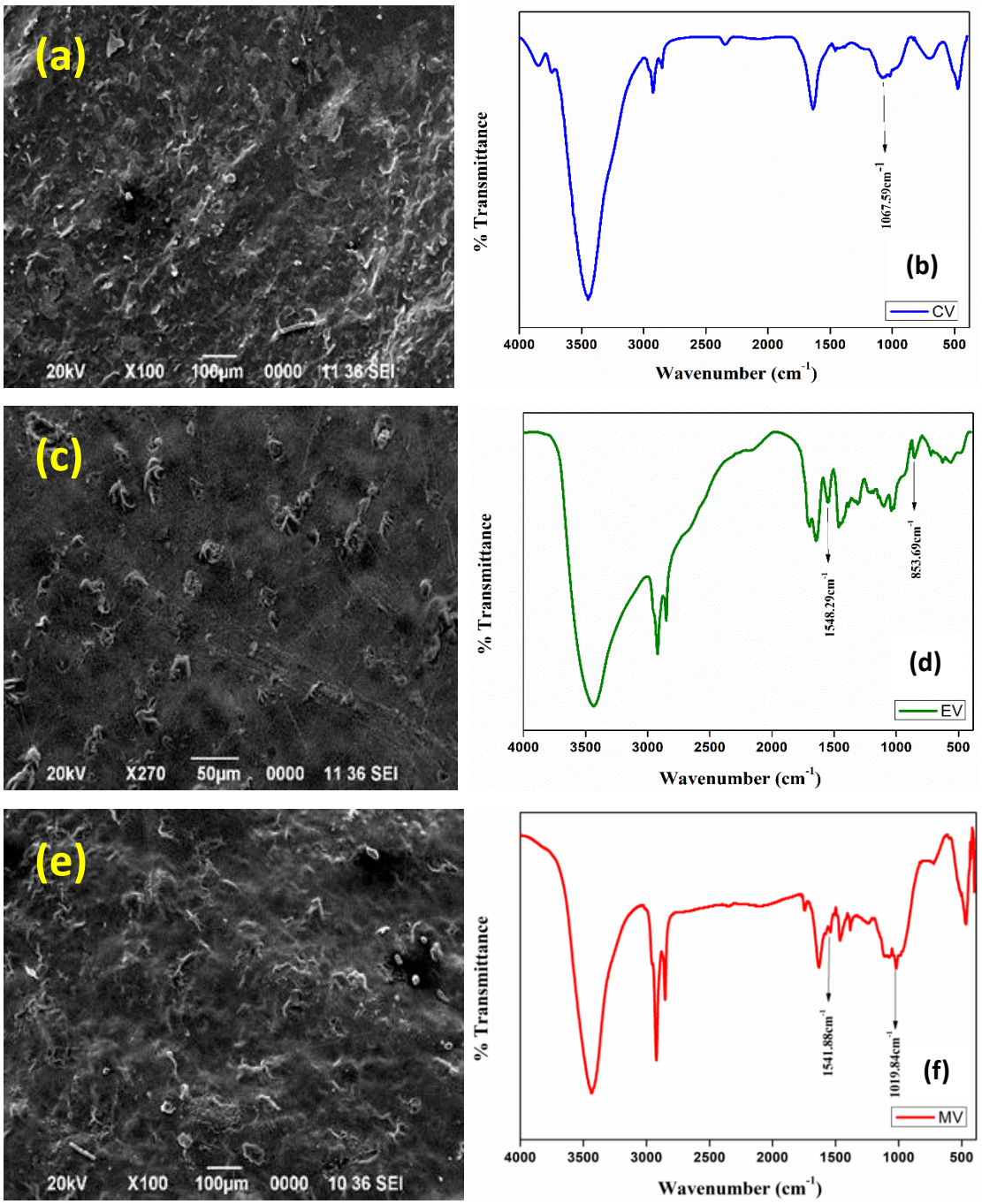

Figure 3.13 SEM images of the adsorbent after removal of (a)CV, (c)EV, (e) MV dye, FT-IR spectra of the adsorbent after dye removal for (b)CV, (d) EV, and (f) MV dye

As can be perceived from the morphological data, the initial structure of the organogel varied from the dye-absorbed SEM images (Figure 3.13 a,c,e). It can be vividly seen that a thick layer has been deposited over the initial surface which is due to the accumulation of dye molecules on the surface of the sorbent. The presence of porous sites acts as an addendum for the entrapment of dye molecules within the sorbent matrix. Significant changes were also observed from the dye-adsorbed FT-IR spectrum (Figure 3.13 b,d,f). Due to the formation of the N–O bond as a result of the interaction between the SO_3^- and $N^+(R_2)$ group of the dye molecules, stretching vibrations occurs around 1550-1540cm^{-1}. The stretching frequency of the S=O and S–O bond also shifts to a lower wavenumber around 1050-850cm^{-1} (based on the three dyes) due to the reaction between the dye and the sorbent.

3.3.3.1 Study of mixed dyes

Dye industrial effluents contain both cationic as well as anionic dyes as their discharge components. Since the prepared sorbent has responded to the adsorption of cationic dyes as per experimental results, an attempt has been made to explore its efficacy in the presence of mixed dyes. Three anionic dyes Congo Red, Eriochrome Black T, and Methyl Orange were used to prepare a binary solution with the most efficient Ethyl Violet dye with a concentration of 10mg/L each mixed in a 1:1 ratio.

Figure 3.14 shows the UV-Vis spectrum of the three different mixed dyes. From the spectra, it can be interpreted that in each of the three cases, the sorbent was completely able to remove cationic dye with partial removal of the anionic species. This can be predicted from the Ethyl Violet – Methyl Orange solution (Figure 3.14c) where the EV was adsorbed up to 97.29% while MO received a removal percentage of 48.64%. While in the case of EV-CR and EV-EBT solutions (Figure 3.14a-b), the removal was not distinguished due to the shifting and merging of the peaks of the mixed dyes. Thus, the sorbent can be termed as a compelling one for the removal of dye effluents from wastewater with an advanced affinity towards cationic dyes.

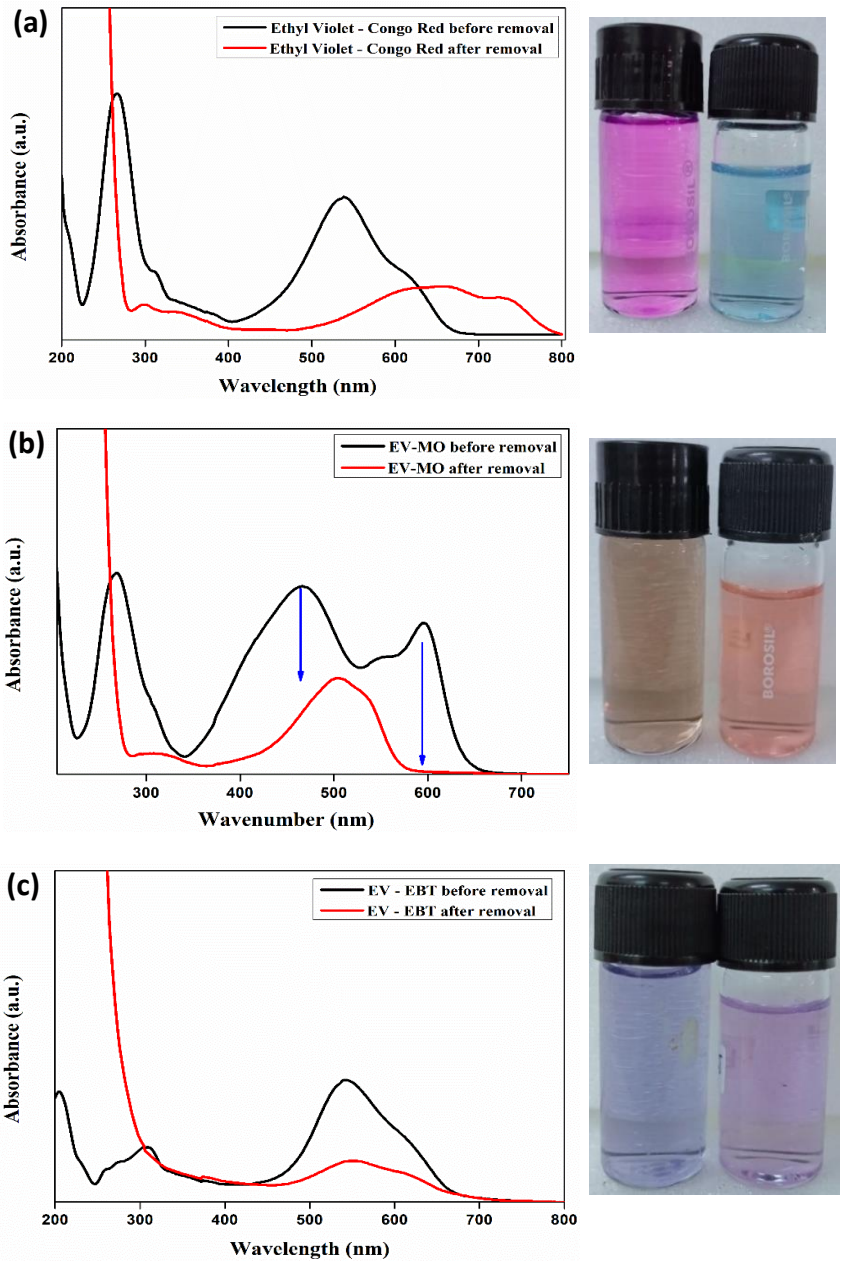

Figure 3.14 UV-Vis spectrum and optical images of the mixed dyes (a) Ethyl Violet-Congo Red, (b) Ethyl Violet-Eriochrome Black T, (c) Ethyl Violet-Methyl Orange before and after adsorption

3.3.3.2 Kinetics of adsorption

The adsorption efficiencies and time dependence of the adsorption process of the respective dyes obtained from the experimental data were evaluated using kinetics models (iii) and (v) of section 2.2.5 in Chapter 2 to study the interaction between sorbent and the dye molecules. Rate constants were studied using plots $\ln(q_e - q_t)$ vs time and t/Qt vs time, where it was observed that the adsorption of the dyes(CV, EV, MV) in plot t/Qt vs time provided a linear fitted relation.

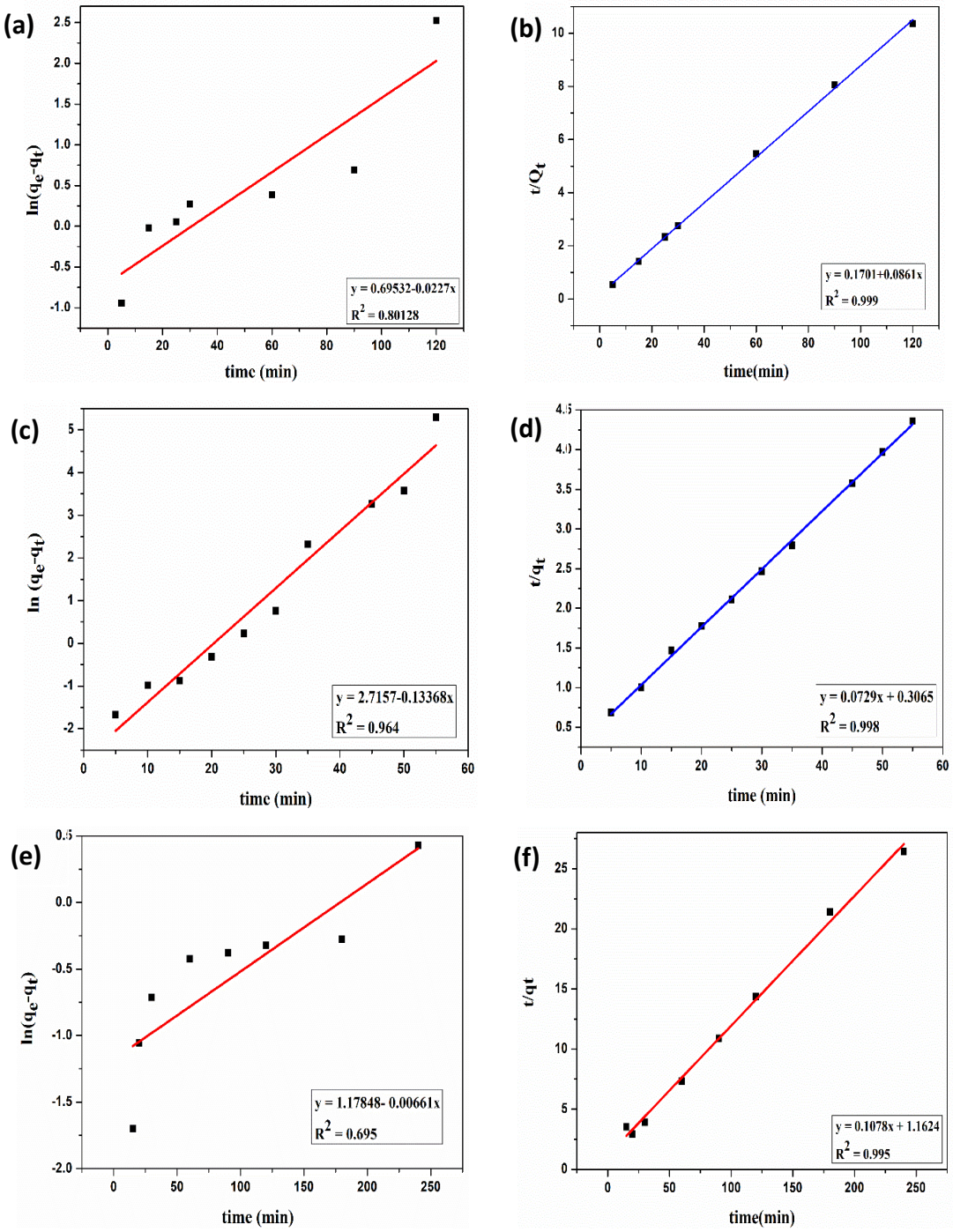

Figure 3.15 First-order kinetics graph (a,c,e) and second-order kinetics graph (b.d.f) for CV, EV, and MV dyes

Thus, it can be conferred that the kinetic and correlation coefficient (R^2) is best suited to the pseudo-second-order model for the adsorption of the dyes onto the sorbent, acting as a rate-limiting step between the sorbent and the dye molecules. The value for regression coefficient (R^2) was seen to be the highest (0.99) for all the three experimented dyes. Hence, kinetic adsorption of cationic dyes was better presaged using second order kinetics model. Attainment of equilibrium sites however proved that all of

the active sites had been fully employed for adsorption by cationic dyes. Fitted kinetics plots for the dyes were displayed in Figure 3.15 while the respective kinetic parameters can be obtained from Table 3.4.

Table 3.4 Kinetic parameters for first and second-order kinetics plot for adsorbed dye

SAMPLE	pseudo-first order-kinetics model		pseudo-second-order-kinetics model		
	$k_1(min^{-1})$	R^2	$k_2(gg^{-1}min^{-1})$	$q_e(gg^{-1})$	R^2
CV	4.63×10^{-3}	**0.80**	8.52×10^{-2}	11.67	**0.99**
EV	2.22×10^{-3}	**0.96**	8.61×10^{-2}	12.38	**0.99**
MV	3.92×10^{-3}	**0.69**	9.79×10^{-2}	9.68	**0.99**

3.3.3.3 Adsorption Isotherm

The interaction action between equilibrium adsorption capacity and equilibrium concentration was evaluated using Langmuir Isotherm, Freundlich Isotherm, and Temkin Isotherm models in their non-linear forms as it furnishes a complicated procedure for determination of kinetic parameters circumventing the complications of linearization (Figure 3.16). The experimental data was plotted using Langmuir, Freundlich, and Temkin isotherms as described in equations (iv),(v) & (vi).

$$C_e/q_e = C_e/q_{max} + 1/K_L \times q_{max} \quad \textbf{(iv)}$$

$$lnq_e = lnK_F + \left(1/n\right)lnC_e \quad \textbf{(v)}$$

$$q_e = BlnK_T + BlnC_e \quad \textbf{(vi)}$$

where, q_e(mg/g) is the amount of dye adsorbed at equilibrium,

q_{max} is the theoretical maximum adsorbed dye

C_e(mg/L) is the equilibrium concentration of dye solution

K_L(L/mg) is the Langmuir isotherm constant

K_F {mg/g.L/mg(1/n)} is the term for Freundlich isotherm where K_F is the adsorption capacity and n is the adsorption intensity.

K_T is the Temkin constant related to the maximum binding energy whereas B is the heat adsorption constant.

The formation of a monolayer on the surface of the adsorbent for maximum adsorption was suggested by Langmuir while Freundlich suggests non-linearity between

adsorbate and concentration of the solution used. The interaction between adsorbate and adsorbent has however been suggested by Temkin.

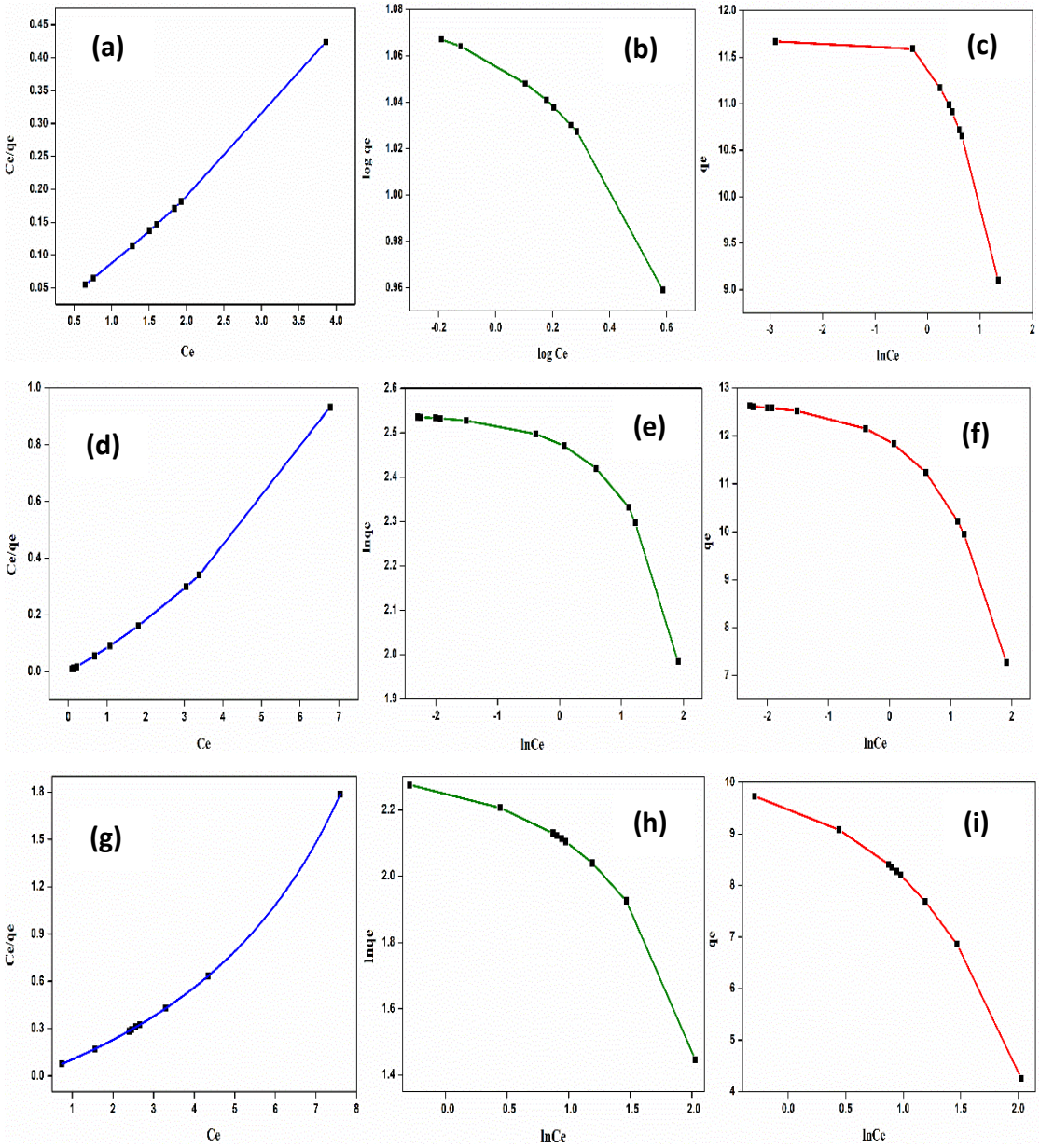

Figure 3.16 The plot of Ce/qe vs Ce (Langmuir) for CV, EV, and MV dyes (a,d,g), the plot of ln qe vs ln Ce (Freundlich) for CV, EV, and MV dyes (b,e,h), the plot of qe vs ln Ce (Temkin) for CV, EV, and MV dyes (c,f, i)

The correlation coefficients (R^2) along with their respective parameters of the proposed isothermic models were obtained from Table 3.5 which, however, suggested that the regression coefficient for the Langmuir model was founded to be close to 1 in comparison to Freundlich and Temkin models in addition to the remarkable fitting of the curve with the experimental data. The results of R^2 and the lower separation factor (R_L) values from Langmuir isotherm suggest that the process of adsorption between sorbent

and dye molecule involves a chemisorption process since the value of $R_L \leq 1$ which effectively describes the better affinity between adsorbate and the sorbent leading to deposition of a monolayer on the surface of the sorbent revealing the presence of strong electrostatic attraction between adsorbent and adsorbate

Table 3.5 Parameters for adsorption isotherms of the respective dyes

ISOTHERMS	PARAMETERS	ADSORBATE		
		CV	EV	MV
LANGMUIR	q_e(mg.g^{-1})	11.67	12.38	9.68
	$K_L \times 10^3$ (L.mg)	3.59	4.05	7.74
	R^2	0.992	0.969	1
	R_L	0.5	0.15	0.56
FREUNDLICH	1/n	0.05	0.04	0.24
	K_F(mg$^{(1-1/n)}$.L$^{1/n}$.g^{-1})	228.3	224.7	200.38
	R^2	0.85	0.66	0.72
TEMKIN	A(L.g^{-1})	1.727	6.46E43	2.25E43
	B	0.127	0.10	0.07
	b_T(J mol^{-1})	17.75	22.63	29.66
	R^2	0.40	0.74	0.82

3.3.3.4 Mass transfer model

The uptake of dyes can be transported from the aqueous phase to the sorbent through the intra-particle diffusion model (viii) of Weber and Morris which is the limiting step for multi-adsorption procedures. The equation can be explained as:

$$q_t = k_{id}\, t^{1/2} + c \qquad \textbf{(vii)}$$

where, k_{id} (mg/g.min $^{-1/2}$) is the rate constant for intraparticle diffusion

c is the intraparticle diffusion constant depicting the boundary layer thickness

$t^{1/2}$ is the time when adsorption of dyes occurs at half equilibrium (obtained from the second-order model

$$t^{1/2} = 1/k_2 q_e \qquad \textbf{(viii)}$$

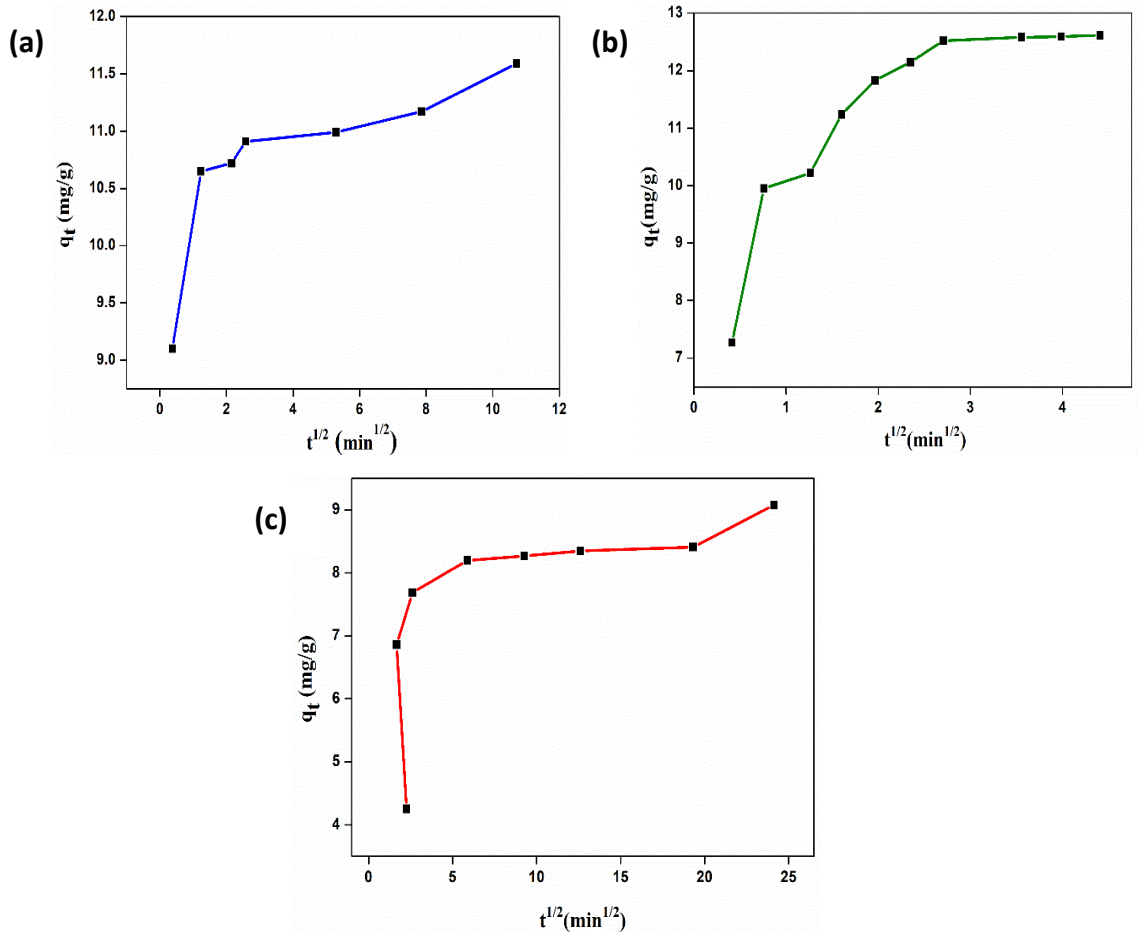

Figure 3.17 The plot of q_t vs $t^{1/2}$ for intra-particle diffusion of (a)CV, (b)EV, and (c)MV dyes

The intake of dyes on the surface of the sorbent was executed using the model as shown in Figure 3.17. It can be interpreted from the diffusion plot of q_t vs $t^{1/2}$ that it exhibited a multi-stage sorption process. In the very first step, a rapid increase has been detected due to the diffusion of the cationic dye molecules from the solution to the external boundary of the sorbent and then to the interior surface through boundary thickness. Meanwhile, the second step denotes the incremental stage of adsorption followed by the third step where with the increase in time, accumulation of molecules occurs at sites lowering the diffusion process until it attains an equilibrium position. As obtained from the three graphs in Figure 3.17, the value for EV was seen to be highest at equilibrium with 12.64mg/g, while 10.71mg/g for CV and 9.1 mg/g for that of MV (which correlates with the value obtained from Table 3.4 for q_e). Parameter C relates to the thickness of the boundary layer; as with the increase in intercept, the boundary layer increases (Table 3.6). The diffusion rate follows the order K_{id} (EV > CV > MV) accordingly with the fast absorbance of the dye onto the sorbent.

Table 3.6 Parameters for diffusion model of the dyes

INTRA-PARTICLE DIFFUSION	PARAMETERS	
	k_{id}	C
CV	0.157	10.05
EV	1.067	8.84
MV	0.119	6.47

Since cationic dyes are conventionally basic dyes, consequently after adsorption of the respective dyes, the adsorbent will be able to emancipate the adsorbed dye on treatment with an acidic solution. Ensuring the drying of the sorbent, it can be again re-used for further adsorption of dyes demonstrating its reusable properties.

3.3.3.5 Mechanism of adsorption

The mechanism for dye adsorption, observed in the experiment is greatly carried out through the chemisorption process as the deposition of monolayer surface can be observed. As observed from Figure 3.18, along with the chemical interactions, there prevails hydrogen bonding between Nitrogen and Hydrogen, Oxygen and Hydrogen, between the aromatic ring of the dye and methyl groups present in the adsorbent which further helps in the swelling/adsorption process.

The most important antecedent for the occurrence of adsorption is the electrostatic interaction between the negatively charged groups of the sorbent with the cationic dye molecule. The mechanism has been discussed in detail for further analysis-

The adsorption process of the sorbent includes three stages for the dyes.

(i) At first, the movement of dyes in the aqueous phase occurs toward the sorbent surface.

(ii) Secondly, the diffusion of dyes from the outer surface through the pores to the inner surface

(iii) Thirdly, the adsorption of dye ensues at the active sites of the sorbent via electrostatic interaction until the attainment of the equilibrium position.

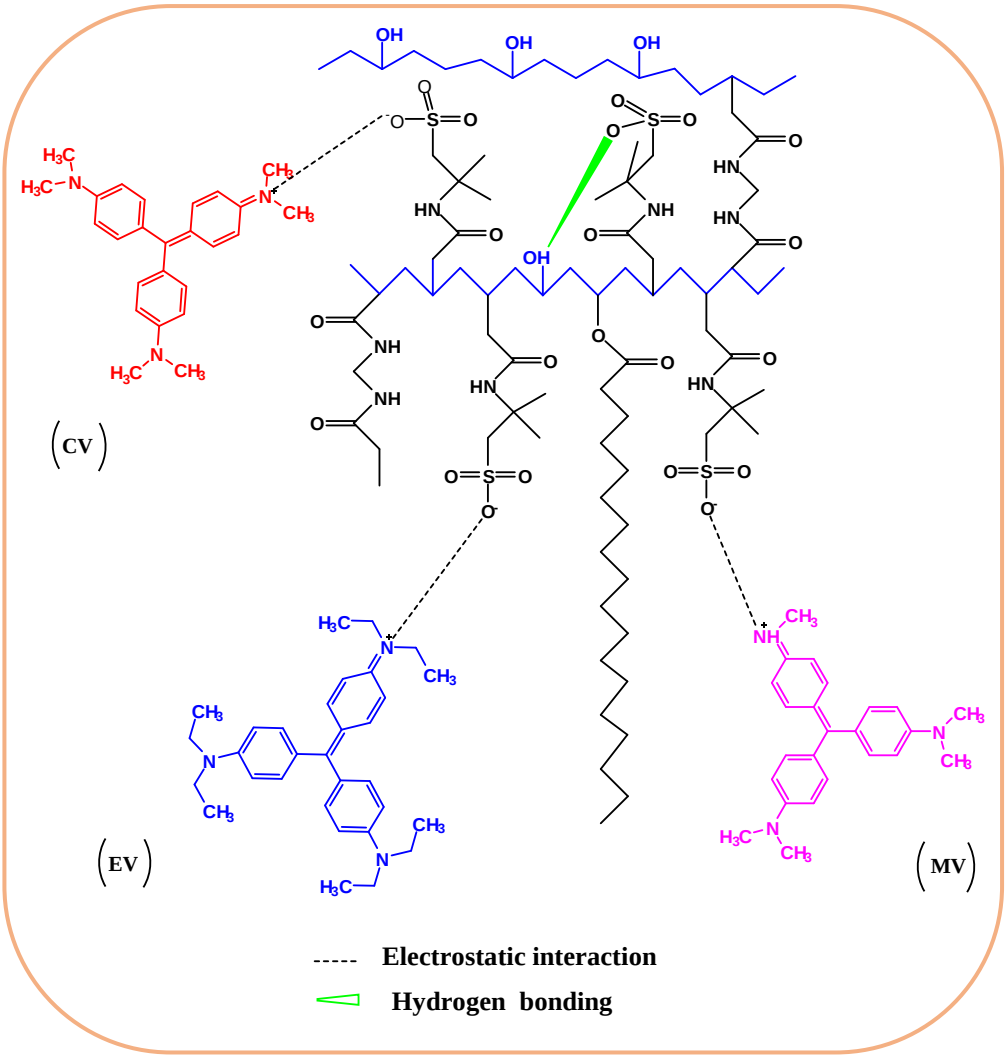

Figure 3.18 Schematic representation for the mechanism of adsorption of dyes CV, EV, MV by the organogel

3.3.3.6 Reusability of organogel

For reasonable claims to be used for industrial purposes, the recyclability and stability of the adsorbent are observed as a substantial factor. Here, a dye solution of 20ppm was prepared and 0.5gm of the sorbent was added to 100 mL of the prepared dye solution of Ethyl Violet. After the adsorption of the dye, the clear solution was analyzed using UV-Vis spectroscopy. The clear solution obtained was decanted while the same sorbent was again used in another 100mL of the dye solution. The cycle was repeated with the same adsorbent about 10 times. From the results obtained in Figure 3.20, it can be observed that the same sorbent was able to clear dye solutions besides the removal percentage was almost the same for around 4 cycles after which a slight decrease was detected which was obvious since the sorbent was used repeatedly for 10 cycles without desorption. However, after the 4th cycle, the duration of adsorption slightly increased between 2-5 hours due to the presence of pre-existed dye molecules. From the attained

results, it can be proven that the solvent can act as a prudent and effectual material for the removal of accumulated cationic dyes and is exceedingly beneficial for its use in industrial sectors.

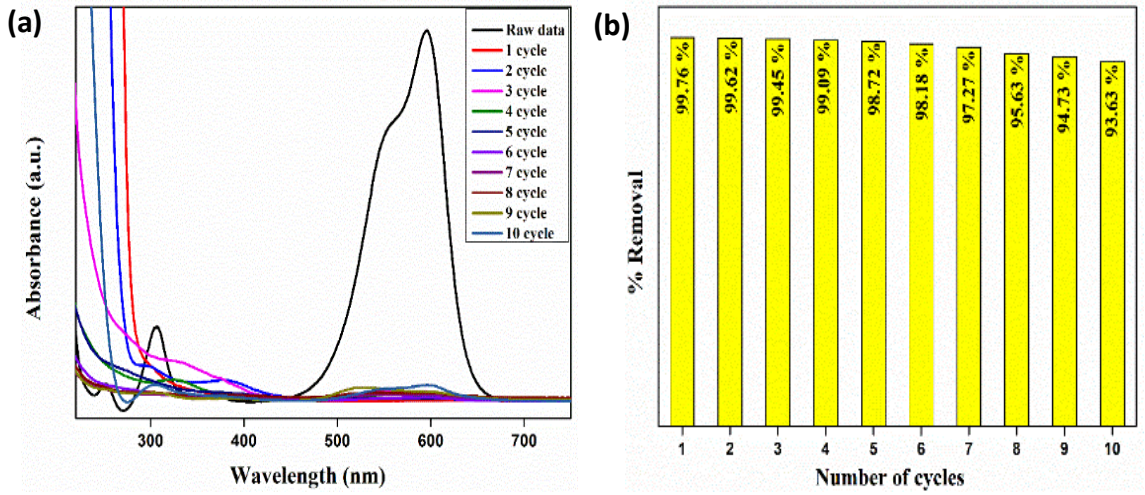

Figure 3.19 (a) UV-Vis spectra and (b) bar plot for the recyclability study of the Ethyl Violet dye

Table 3.7 A comparative study of the dyes using different gel-based adsorbents

Gel adsorbents	Dye used	Contact time	Removal %	Reference
Glutamic acid-derived organogel	CV	24hr	99	[50]
Low Molecular Weight amphiphilic dipeptides	CV	24hr	97%	[51]
Acrylic acid-hydroxyethyl acrylate polymer	MV	30hr	67	[52]
Sodium acrylate-hydroxyethyl methacrylate polymer			80	
Acrylic acid-hydroxyethyl methacrylate-Na alginate				
Sodium acrylate-hydroxyethyl methacrylate-Na alginate			90	
			95	
Terpyridine-based smart hybrid gel	CV	30hr	94.2	[53]
Catechol-based metal-organic gels	MV	3hr	93.99	[54]
Bidirectionally zwitterionic polymer hydrogel	MV	24hr	10	[55]
Pectin-based ZnO-g-copolymer hybrid nanocomposite	CV	2hr	95.7	[38]
Low molecular weight gelator grafted polymeric organogel	EV	1hr	99.35	This work
	CV	2.5hr	95.06	
	MV	5hr	92.71	

3.4 CONCLUSION

The current study focuses on the synthesis of an organogel with excellent absorption and adsorption properties. The incorporation of AMPS into the gel structure created active sites, which not only facilitated cross-linking but also resulted in the formation of pores, thereby enhancing the adsorption capacity. The gel exhibited an impressive solvent absorption capacity, reaching nearly 10 times its initial weight, and demonstrated efficient solvent reusability for up to 10 cycles. In terms of adsorption, the gel selectively adsorbed cationic dyes from polluted water sources, achieving maximum adsorption capacities of 12.38 mg/g, 11.67 mg/g, and 9.68 mg/g for ethyl violet dye, crystal violet, and methyl violet dyes, respectively. Moreover, the gel displayed remarkable removal efficiencies of 99.35%, 95.06%, and 92.71% for ethyl violet dye, crystal violet, and methyl violet dyes, respectively, within different time intervals of 60 minutes, 150 minutes, and 300 minutes.

The sorption process followed the kinetic behavior described by the pseudo-second-order model, while the Langmuir adsorption isotherm was applicable, indicating the formation of a monolayer of adsorbate particles through chemisorption. Additionally, the sorption process was influenced by time-dependent intra-particle diffusion, which was identified as one of the rate-determining steps. The primary mechanism of adsorption involved electrostatic interactions between the adsorbent and adsorbate molecules, as well as dipole-induced dipole interactions. The sorbent exhibited effective removal of 97.29% of Ethyl Violet and 48.64% of Methyl Orange from a mixed dye solution. Furthermore, the sorbent displayed the potential for repeated use without undergoing a desorption procedure, allowing for its application in solvent removal and the effective removal of harmful dyes from contaminated water sources.

3.5 REFERENCES

[1] Singh, K., Kumar, P., and Srivastava, R. An overview of Textile Dyes and their Removal Techniques: Indian Perspective. *Pollution Research*, 36 (4): 790–797, 2017.

[2] Dutta, S., Gupta, B., Srivastava, S. K., and Gupta, A. K. Recent Advances on the Removal of Dyes from Wastewater Using Various Adsorbents: A Critical Review. *Materials Advances*, 2 (14): 4497–4531, 2021.

[3] Desore, A., and Narula, S. A. An Overview on Corporate Response towards Sustainability Issues in Textile Industry. *Environment, Development and Sustainability*, 20 (4): 1439–1459, 2018.

[4] Hegde, V., Uthappa, U. T., Arvind Swami, O. R., Han, S. S., Jung, H. Y., Altalhi, T., and Kurkuri, M. D. Sustainable Green Functional Nano Aluminium Fumarate-MOF Decorated on 3D Low-Cost Natural Diatoms for the Removal of Congo Red Dye and Fabric Whitening Agent from Wastewater: Batch & Continuous Adsorption Process. *Materials Today Communications*, 32, 103887, 2022.

[5] Chequer, F. M. D, Oliveira, G. A. R., Ferraz, E. R. A.; Cardoso, J. C., Zanoni, M. V. B., and Oliveir, D. P. Textile Dyes: Dyeing Process and Environmental Impact. In *Eco-Friendly Textile Dyeing and Finishing*, ISBN: 978-953-51-0892-4. InTechOpen, 2013.

[6] Bafana, A., Devi, S. S., and Chakrabarti, T. Azo Dyes: Past, Present and the Future. *Environmental Reviews*, 19 (1): 350–370, 2011.

[7] Forgacs, E., Cserháti, T., and Oros, G. Removal of Synthetic Dyes from Wastewaters: A Review. *Environmental International*, 30 (7): 953–971, 2004.

[8] Przystas, W., Zablocka-Godlewska, E., and Grabinska-Sota, E. Biological Removal of Azo and Triphenylmethane Dyes and Toxicity of Process By-Products. *Water, Air, & Soil Pollution*, 223 (4): 1581–1592, 2012.

[9] Karpińska, J., and Kotowska, U. Removal of Organic Pollution in the Water Environment. *Water*, 11 (10), 2017.

[10] Huang, R., McPhedran, K. N., Sun, N., Ayala, P. C., and Gamal El-Din, M. Investigation of the Impact of Organic Solvent Type and Solution PH on the Extraction Efficiency of Naphthenic Acids from Oil Sands Process-Affected Water. *Chemosphere*, 146: 472–477, 2016.

[11] Joshi, D. R., and Adhikari, N. An Overview on Common Organic Solvents and Their Toxicity. *Journal of Pharmaceutical Research International*, 28 (3): 1–18, 2019.

[12] Tian, M., Fang, L., Yan, X., Xiao, W., and Row, K. H. Determination of Heavy Metal Ions and Organic Pollutants in Water Samples Using Ionic Liquids and Ionic Liquid-Modified Sorbents. *Journal of Analytical Methods in Chemistry*, 1948965, 2019.

[13] Fallahzadeh, R. A., Khosravi, R., Dehdashti, B., Ghahramani, E., Omidi, F., Adli, A., and Miri, M. Spatial Distribution Variation and Probabilistic Risk Assessment of Exposure to Chromium in Ground Water Supplies; a Case Study in the East of Iran. *Food and Chemical Toxicology*, 115, 260–266, 2018.

[14] Ossai, I. C., Ahmed, A., Hassan, A., and Hamid, F. S. Remediation of Soil and Water Contaminated with Petroleum Hydrocarbon: A Review. *Environmental Technology & Innovation*, 17, 100526, 2020.

[15] Truskewycz, A., Gundry, T. D., Khudur, L. S., Kolobaric, A., Taha, M., Medina, A. A., Ball, A. S., and Shahsavari, E. Petroleum Hydrocarbon Contamination in Terrestrial Ecosystems—Fate and Microbial Responses. *Molecules*, 24 (18), 3400, 2019.

[16] Maiques, F. J. O., Garcia, A. I. R., Puerto, J. M., Cano, J. A. B., and Cases, F. Electrochemical Treatment of Real Textile Wastewater: Trichromy Procion HEXL®. *Journal of Electroanalytical Chemistry*, 808: 387–394, 2018.

[17] Lellis, B., Fávaro-Polonio, C. Z., Pamphile, J. A., and Polonio, J. C. Effects of Textile Dyes on Health and the Environment and Bioremediation Potential of Living Organisms. *Biotechnology Research and Innovation*, 3 (2): 275–290, 2019.

[18] Hassan, M. M., and Carr, C. M. A Critical Review on Recent Advancements of the Removal of Reactive Dyes from Dyehouse Effluent by Ion-Exchange Adsorbents. *Chemosphere*, 209: 201–219, 2018.

[19] Marchetti, P., Maria, F., Solomon, J., Szekely, G., and Livingston, A. G. Molecular Separation with Organic Solvent Nanofiltration: A Critical Review. *Chemical Reviews*, 114 (21): 10735–10806, 2014.

[20] Wei, Y., Cheng, X., Ding, A., and Xu, J. Magnesium Silicate Polymer as a Coagulant for Reactive Dye Removal from Wastewater: Considering the Intrinsic PH in Magnesium Silicate Polymer and Coagulation Behavior. *ACS Omega*, 5 (40): 26094–26100, 2020.

[21] Barros, G. K. G. C.; Duarte, L. J. N., Melo, R. P. F., Lopes, F. W. B., and Neto, E. L. B. Ionic Dye Removal Using Solvent-Assisted Ionic Micellar Flocculation. *Journal of Polymers and the Environment*, 30 (6): 2534–2546, 2022.

[22] Li, W., Zhang, Y., Liu, T., Huang, J., and Wang, Y. Comparison of Ion Exchange and Solvent Extraction in Recovering Vanadium from Sulfuric Acid Leach Solutions of Stone Coal. *Hydrometallurgy*, 131–132: 1–7, 2013.

[23] Pillai, I. M. S., and Gupta, A. K. Effect of Inorganic Anions and Oxidizing Agents on Electrochemical Oxidation of Methyl Orange, Malachite Green and 2,4-Dinitrophenol. *Journal of Electroanalytical Chemistry*, 762: 66–72, 2016.

[24] Sriram, G., Uthappa, U. T., Kigga, M., Jung, H. Y., Altalhi, T., Brahmkhatri, V., and Kurkuri, M. D. Xerogel Activated Diatoms as an Effective Hybrid Adsorbent for the Efficient Removal of Malachite Green. *New Journal of Chemistry*, 43 (9): 3810–3820, 2019.

[25] Uthappa, U. T., Bhat, S., Soo Han, S., Jeong, H. H., Altalhi, T., Jung, H. Y., and Kurkuri, M. D. Tailoring of 2D MoS2 Microspheres on 3D Low-Cost DE for the Efficient Removal of Hazardous Cationic Dyes. *Advanced Powder Technology*, 33 (11), 103800, 2022.

[26] Sahoo, C., and Gupta, A. K. Photocatalytic Degradation of Methyl Blue by Silver Ion-Doped Titania: Identification of Degradation Products by GC-MS and IC Analysis. *Journal of Environmental Science and Health Part A Toxic Hazardous Substances & Environmental Engineering*, 50 (13): 1333–1341, 2015.

[27] Gupta, A. K., Pal, A., and Sahoo, C. Photocatalytic Degradation of a Mixture of Crystal Violet (Basic Violet 3) and Methyl Red Dye in Aqueous Suspensions Using Ag+ Doped TiO2. *Dyes and Pigments*, 69 (3): 224–232, 2006.

[28] Saravanan, R., Gracia, F., and Stephen, A. Basic Principles, Mechanism, and Challenges of Photocatalysis. In: Khan, M., Pradhan, D., Sohn, Y. (eds) *Nanocomposites for Visible Light-induced Photocatalysis*, pages 19–40, ISBN: 978-3-319-62446-4. Polymer and Composite Materials, 2017.

[29] Iervolino, G., Zammit, I., Vaiano, V., and Rizzo, L. Limitations and Prospects for Wastewater Treatment by UV and Visible-Light-Active Heterogeneous Photocatalysis: A Critical Review. *Topics in Current Chemistry*, 378 (1): 7, 2020.

[30] Lim, J. Y. C., Goh, S. S., Liow, S. S., Xue, K., and Loh, X. J. Molecular Gel Sorbent Materials for Environmental Remediation and Wastewater Treatment. *Journal of Materials Chemistry A*, 7 (32): 18759–18791, 2019.

[31] Yati, I., Aydin, G. O., and Sonmez, H. B. Cross-Linked Poly (Tetrahydrofuran) as Promising Sorbent for Organic Solvent/Oil Spill. *Journal of Hazardous Materials*, 309: 210–218, 2016.

[32] Yati, I., Karadag, K., and Sonmez, H. B. Amphiphilic Poly (Ethylene Glycol) Gels and Their Swelling Features. *Polymers for Advanced Technologies*, 26 (6): 635–644, 2015.

[33] Gisi, S. D., Lofrano, G., Grassi, M., and Notarnicola, M. Characteristics and Adsorption Capacities of Low-Cost Sorbents for Wastewater Treatment: A Review. *Sustainable Materials and Technologies*, 9: 10–40, 2016.

[34] Zhao, B., Rohm, K., Wang, F., Gong, X., Zloczower, I. M. and Feke, D. L. A Compact Volume-Expandable Sorbent for Oil and Solvent Capture. *ACS Applied Polymer Materials*, 3 (1): 494–503, 2021.

[35] Hegde, V., Uthappa, U. T., Suneetha, M., Altalhi, T., Soo Han, S., and Kurkuri, M. D. Functional Porous Ce-UiO-66 MOF@Keratin Composites for the Efficient Adsorption of Trypan Blue Dye from Wastewater: A Step towards Practical Implementations. *Chemical Engineering Journal*, 461, 142103, 2023.

[36] Hu, X. S., Liang, R., and Sun, G. Super-Adsorbent Hydrogel for Removal of Methylene Blue Dye from Aqueous Solution. *Journal of Materials Chemistry A*, 6 (36): 17612–17624, 2018.

[37] Mahdavinia, G. R., Aghaie, H., Sheykhloie, H., Vardini, M. T., and Etemadi, H. Synthesis of CarAlg/MMt Nanocomposite Hydrogels and Adsorption of Cationic Crystal Violet. *Carbohydrate Polymers*, 98 (1): 358–365, 2013.

[38] Kodoth, A. K., and Badalamoole, V. Pectin Based Graft Copolymer–ZnO Hybrid Nanocomposite for the Adsorptive Removal of Crystal Violet. *Journal of Polymers and the Environment*, 27 (9): 2040–2053, 2019.

[39] Bhat, S., Uthappa, U. T., Sadhasivam, T., Altalhi, T., Soo Han, S., and Kurkuri, M. D. Abundant Cilantro Derived High Surface Area Activated Carbon (AC) for Superior

Adsorption Performances of Cationic/Anionic Dyes and Supercapacitor Application. *Chemical Engineering Journal*, 459, 141577, 2023.

[40] Srivastava, A., Gupta, B., Majumder, A., Gupta, A. K., and Nimbhorkar, S. K. A Comprehensive Review on the Synthesis, Performance, Modifications, and Regeneration of Activated Carbon for the Adsorptive Removal of Various Water Pollutants. *Journal of Environmental Chemical Engineering*, 9 (5), 106177, 2021.

[41] Das, S., Chakraborty, P., Ghosh, R., Paul, S., Mondal, S., Panja, A., and Nandi, A. K. Folic Acid-Polyaniline Hybrid Hydrogel for Adsorption/Reduction of Chromium (VI) and Selective Adsorption of Anionic Dye from Water. *ACS Sustainable Chemistry & Engineering*, 5 (10): 9325–9337, 2017.

[42] Wang, L., Wu, X., Xu, W., Huang, X., Liu, J., and Xu, A. Stable Organic − Inorganic Hybrid of Polyanilineα-Zirconium.Phosphate for Efficient Removal of Organic Pollutants in Water Environment. *ACS Applied Materials & Interfaces*, 4 (5): 2686–2692, 2012.

[43] Pan, A., Roy, S. G., Haldar, U., Mahapatra, R. D., Harper, G. R., Low, W. L., De, P., and Hardy, J. G. Uptake and Release of Species from Carbohydrate Containing Organogels and Hydrogels. *Gels*, 5 (4), 43, 2019.

[44] Ren, S., Sun, P., Wu, A., Sun, N., Sun, L., Dong, B., and Zheng, L. Ultra-Fast Self-Healing PVA Organogels Based on Dynamic Covalent Chemistry for Dye Selective Adsorption. *New Journal of Chemistry*, 43 (20): 7701–7707, 2019.

[45] Baruah, K., Ahmed, A., Dutta, R., Ahmed, S., Lahkar, S., and Dolui, S. K. Removal of Organic Solvents from Contaminated Water Surface through a Fatty Acid Grafted Polyvinyl Alcohol Based Organogel. *Journal of Applied Polymer Science*, 139 (45), e53123, 2022.

[46] Okesola, B. O., and Smith, D. K. Applying Low-Molecular Weight Supramolecular Gelators in an Environmental Setting-Self-Assembled Gels as Smart Materials for Pollutant Removal. *Chemical Society Reviews*, 45 (15): 4226-4251, 2016.

[47] Zheng, X., Zheng, H., Zhao, R., Xiong, Z., Wang, Y., Sun, Y., and Ding, W. Sulfonic Acid-Modified Polyacrylamide Magnetic Composite with Wide PH Applicability for

Efficient Removal of Cationic Dyes. *Journal of Molecular Liquids*, 319, 114161, 2020.

[48] Modrogan, C., Căprărescu, S., Dăncilă, A. M., Orbuleț, O. D., Grumezescu, A. M., Purcar, V., Radițoiu, V., and Fierascu, R. C. Modified Composite Based on Magnetite and Polyvinyl Alcohol: Synthesis, Characterization, and Degradation Studies of the Methyl Orange Dye from Synthetic Wastewater. *Polymers*, 13 (22), 3911, 2021.

[49] Kodoth, A. K., and Badalamoole, V. Silver Nanoparticle-Embedded Pectin-Based Hydrogel for Adsorptive Removal of Dyes and Metal Ions. *Polymer Bulletin*, 77 (2): 541–564, 2020.

[50] Sar, P., Roy, S. G., De, P., and Ghosh, S. Synthesis of Glutamic Acid Derived Organogels and Their Applications in Dye Removal from Aqueous Medium. *Macromolecular Materials and Engineering*, 305 (4), 1900809, 2020.

[51] Kar, T., Debnath, S., Das, D., Shome, A., and Das, P. K. Organogelation and Hydrogelation of Low-Molecular-Weight Amphiphilic Dipeptides: PH Responsiveness in Phase-Selective Gelation and Dye Removal. *Langmuir*, 25 (15): 8639–8648, 2009.

[52] Mandal, B., and Ray, S. K. Synthesis of Interpenetrating Network Hydrogel from Poly (Acrylic Acid-Co-Hydroxyethyl Methacrylate) and Sodium Alginate: Modeling and Kinetics Study for Removal of Synthetic Dyes from Water. *Carbohydrate Polymers*, 98 (1): 257–269, 2013.

[53] Cho, E. J., Jeong, I. Y., Lee, S. J., Han, W. S., Kang, J. K., and Jung, J. H. Terpyridine-Based Smart Organic-Inorganic Hybrid Gel as Potential Dye-Adsorbing Agent for Water Purification. *Tetrahedron Letters*, 49 (6): 1076–1079, 2008.

[54] Hong, Y., Gao, Z., Chen, M., Hao, J., and Dong, S. Metal-Organic Gels of Catechol-Based Ligands with Ni(II) Acetate for Dye Adsorption. *Langmuir*, 34 (32): 9435–9441, 2018.

[55] Wei, R., Song, W., Yang, F., Zhou, J., Zhang, M., Zhang, X., Zhao, W., and Zhao, C. Bidirectionally PH-Responsive Zwitterionic Polymer Hydrogels with Switchable Selective Adsorption Capacities for Anionic and Cationic Dyes. *Industrial & Engineering Chemistry Research*, 57 (24), 8209–8219, 2018.

CHAPTER 3

SECTION (B)

Polymeric organogel as an effective approach for removal of heavy metal ions from water through adsorption stratagem

This chapter describes the eradication of heavy metal ions present in polluted sources through surface assimilation.

This part of the thesis is published in

Baruah, K., Dutta, R., Doley, S., Sarma, B., and Dolui, S.K. Polymeric organogel as an effective approach for eradication of heavy metal ions As, Pb, Cd, and Cr from the surface of groundwater through adsorption stratagem. ***Journal of Applied Polymer Science***, 141 (2), 2024

3.6 INTRODUCTION

Water is a crucial resource for all life forms on Earth, with its primary sources being surface water and underground water. Surface water, which includes sea, river, and rainwater, mainly contains sulphates and bicarbonates. On the other hand, underground water sources such as spring and well water mostly contain salts in their dissolved state. The increase in industrialization has led to serious environmental concerns regarding the discharge of water containing heavy metal ions by heavy industries [1–3]. This water is unsuitable for drinking or agricultural purposes. When these metal ions come into contact with the water surface, they are converted into sulphates and carbonates and eventually get adsorbed by organic sediments [4].

The discharge of metal ions can occur through direct pollution, such as soil contamination, or indirect pollution through water or air. The major sources of metal ion release include natural occurrences like volcanic eruptions and aerosols, agricultural activities involving the use of fertilizers, pesticides, and sewage sludges, industrial processes such as mining, refineries, and ores, as well as domestic activities like e-waste disposal and biomass burning. Medical disposables also contribute to the release of metal ions. Heavy metals commonly found in water include Arsenic, Cadmium, Lead, Chromium, Tin, and Mercury. Arsenic, particularly in the form of arsenite As(III), is highly toxic as it inhibits enzymatic action in the body [5]. Metallic lead readily oxidizes when in contact with water and transforms into trialkyl lead upon absorption by the body, leading to chronic immune diseases, metabolic disorders, and severe organ damage [6]. Lead can also replace zinc and calcium in the body, causing harmful consequences. Chromium [7] and cadmium [8] exposure can result in cardiovascular and hematological effects, as well as immunological disorders. Mercury and tin compounds undergo active methylation processes, further complicating the deteriorating biological systems of living organisms.

Attempts have been made using conventional methods such as membrane filtration [9], ion exchange method [10], Fenton reagent method [11], coagulation [12], and chemical precipitation [13] for metal ion removal; yet, there seem to be certain disadvantages in the existing methods due to which adsorption method [14–17] has proved to be one of the most effective yet productive techniques with easy preparation procedure for removal of heavy metal ions from aquatic sources while providing sites for binding metallic ions.

Studies on the removal of heavy metal have been carried out using membrane [18], hydrogel [19–21], through green synthesis [22], aerogel [23], metal-organic frameworks (MOF) [24], double network gels [25,26], coagulation [27], fixed bed process [28], carbon-based material [8]. Jing Chen and group reported an adsorbent based on hydrogel capable of adsorbing Pb^{2+} ions through polymerization using acrylic acid and 2-hydroxyethylmethacrylate [19]. Lau Kia Kian et.al. through vapour-induced phase inversion method prepared membrane composed of poly(butylene succinate) and poly(butylene adipate-co-terepthalate) with nanocrystalline cellulose for removal of Cr(III) and Mn(II) ions[18]. M'hamed and co prepared a pyrimidine derived adsorbent using planetary ball mill method for adsorption of Cu(II) ions from aqueous system [22]. Removal of uranium was carried out using different metal oxide aerogels developed by Jun Liao and group using chitosan and some rare earth elements [23]. Lin Chu et.al. reported a double network gel composed of polyvinyl alcohol and polyacrylic acid for removal of Pb(II) and Cd(II) from wastewater resources [25]. Kobielska and group reported metal-organic frameworks as effective material for removal of metallic pollutants from water surfaces [24]. Lerthai.C. studied the removal of certain transition metals using coagulation and precipitation procedure [27]. W.Kong and co reported a graft polymerization between carbon based material graphene oxide and polyacrylic acid for effective adsorption of Cd(II) from wastewater also utilized as photocatalyst [8]. Zhou and group prepared a porous double network jute-polyacrylic acid based gel for removing industrial effluents using fixed bed process [28]. Godiya et.al. reported a bio-based bilateral hydrogel with affinity for Cu(II), Pb(II), and Cd(II) ions for treatment of wastewater using CMC and polyacrylamide [21]. The use of δ-radiation has been carried out for removal of metal ions Cr(III) and Pb(II) by Hong group[20]. J.Ma and co utilized a humic substance based hydrogel by radical polymerization for removal of Pb, Cu, Cd ions in individual as well as multicomponent system for treatment of metal polluted water system [26].

The utilization of polymer materials in the form of organogels for the removal or adsorption of metal ions from metal-contaminated surfaces has been sparsely documented in the literature. The significance of this research lies in the application of gelators. Our efforts aim to contribute to the promotion of a sustainable environment through the adsorption of heavy metals in groundwater, achieved by the interaction between the active sites of the organogel and the metal ions. The choice of a gel as an

adsorbent is based on its recyclability, quick synthesis, biodegradability, and non-toxic nature, which make it a promising candidate for the removal of metallic pollutants from water. Previous studies have already demonstrated the effectiveness of the organogel as an adsorbent by successfully removing cationic dyes and solvents [29]. In this study, the focus is solely on the removal of heavy metals from aqueous solutions, without generating any secondary pollutants. This demonstrates the efficacy of the adsorbent in creating a cleaner and sustainable environment by establishing a strong interactive force between the active sites of the adsorbent and the metal ions. The presence of functional sites is of paramount importance, as they provide the necessary binding sites for the removal of the target species.

The prepared sorbent possesses sulfonic acid groups at its active sites, which, upon neutralization, form sulfonate groups responsible for the successful binding and adsorption of toxic heavy metal ions found in groundwater, such as Arsenite, Lead, Cadmium, and Chromium. The presence of these metal ions was confirmed through SEM images of the adsorbent, along with the identification of the respective metals using SEM-EDX analysis. Additionally, stearic acid enhances the hydrophobic characteristics of the sorbent, enabling its application in aqueous solutions with high adsorption capacity, facilitated by a cross-linking group. To accurately depict the adsorption mechanism of the sorbent, the order of kinetics, adsorption isotherms, and the diffusion model of mass transfer were investigated.

3.7 EXPERIMENTAL SECTION:

3.7.1 Materials:

Materials used for organogel preparation were similar to those mentioned in Section 3.2.1. Copper oxide and Chromium nitrate nonahydrate were purchased from Sigma-Aldrich. Dimethyl sulfoxide (DMSO), Cadmium chloride, Cobalt chloride, and Nickel sulphate were procured from Merck while SDS chemicals provided Lead oxide respectively. The reagents and chemicals used were all of the analytical grades and used as received.

3.7.2 Preparation of the organogel:

Preparation of the organogel was similar as mentioned in Section 3.2.2

3.7.3 Characterization:

Characterization of the formed organogel has been discussed in Section 3.2.3 The determination of metal adsorbed by the sorbent was investigated using an iCE 3500 Thermoscientific Atomic Absorption Spectrophotometer. To detect the presence of elements after adsorption by the gel, XPS analysis was performed.

The organogel was used for the removal of groundwater heavy metal pollutants. For this purpose, Arsenic trioxide, Lead oxide, Cadmium chloride monohydrate, and Chromium nitrate nonahydrate have been prepared in a water solution separately for each of the metals. The percentage of removal efficiency R_e (%) for the adsorbed metal ions was determined by the equation

$$\mathbf{R_e\ (\%) = 1\ - C_f/C_i\ \times 100} \qquad \textbf{(i)}$$

where C_i is the initial and C_f is the final concentration respectively

The capacity of adsorption (Q_e) of the metal ions from metal-contaminated water surface was calculated using

$$\mathbf{Q_e(mg/g) = C_i\ -\ C_f \times\ V/W} \qquad \textbf{(ii)}$$

W(g) is the weight of the used adsorbent and V(L) is the amount of solution used

The kinetic study for the removal of each of the heavy metals was carried out to determine the adsorption rate every 60 minutes for 5 hours. Accordingly, isothermal studies with a mass transfer diffusion model were also carried out to accurately determine the adsorption mechanism.

3.8 RESULTS & DISCUSSION

3.8.1 Morphological and EDX analysis

The bare surface of the organogel prepared has active sites that possess the ability to adsorb metal ions effectively from contaminated water sources. The adsorption process results in the deposition of metal ions over the entire surface of the adsorbent. SEM images (Figure 3.20) obtained after the adsorption procedure are indicative of the highly efficient adsorption capacity of the organogel. Moreover, EDX data (Figure 3.21) further validate the successful adsorption of metal ions onto the sorbent. This indicates that the prepared organogel can be utilized as an effective sorbent for the removal of metal ions from contaminated water sources.

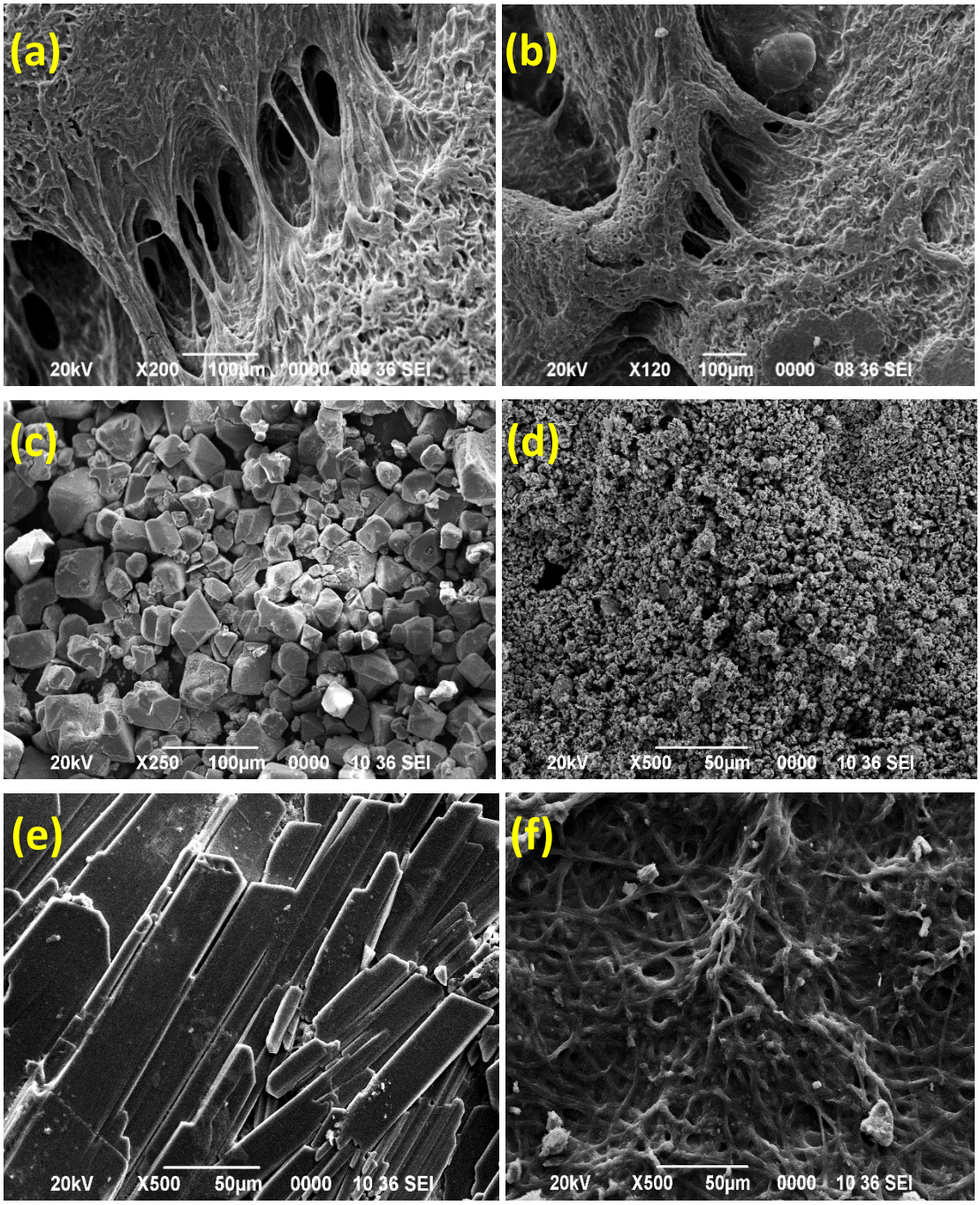

Figure 3.20 Morphological images of the bare organogel surface (a-b), surface after adsorption by metal ions Arsenic(c), Lead(d), Cadmium (e) and Chromium (f) from aqueous surfaces

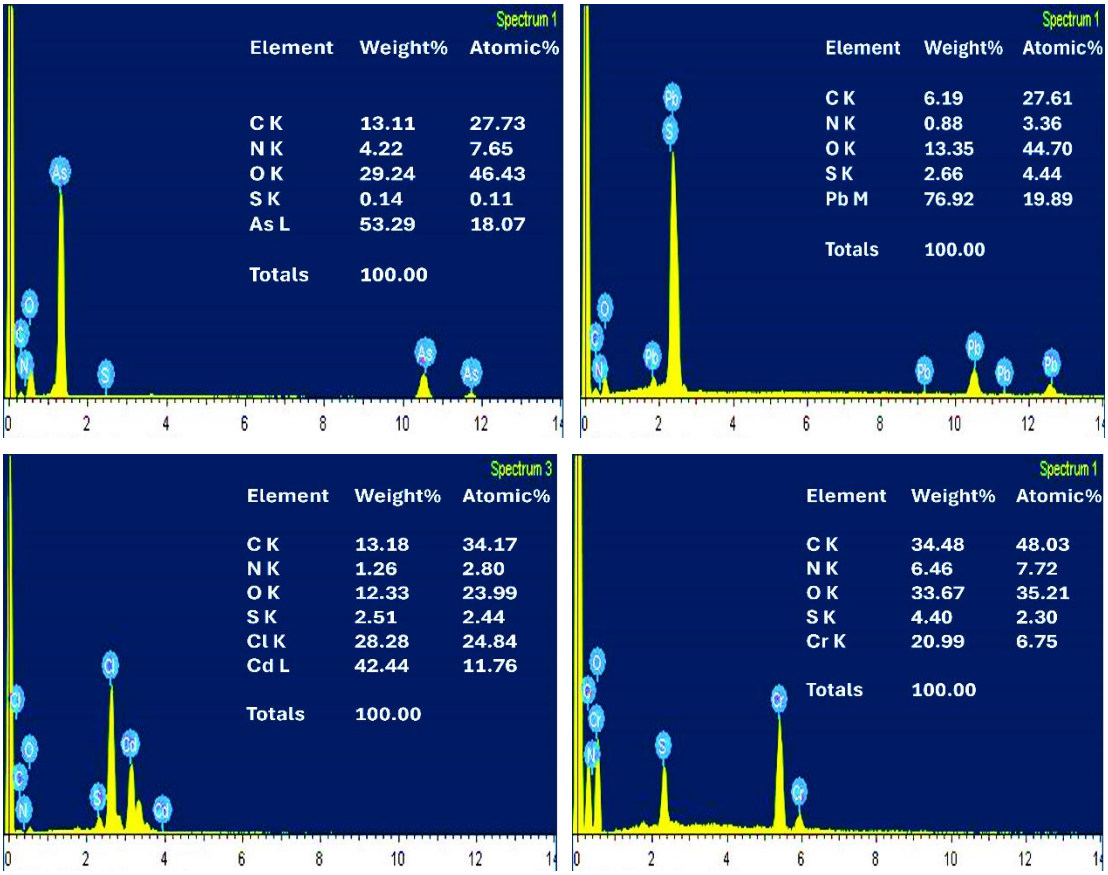

Figure 3.21 SEM-EDX analysis of the adsorbed metal ions onto the organogel

3.8.2 FT-IR analysis

FT-IR spectra (Figure 3.22) denote the attachment/presence of arsenic with the increase in shifting of peaks around 797.89cm⁻1 [39,40], of lead around 682.4cm⁻1 [41], cadmium around 531.94cm⁻1 [42], 944.60cm⁻1 [43] and chromium around 642.87cm⁻1 [44] thus providing evidence to our work.

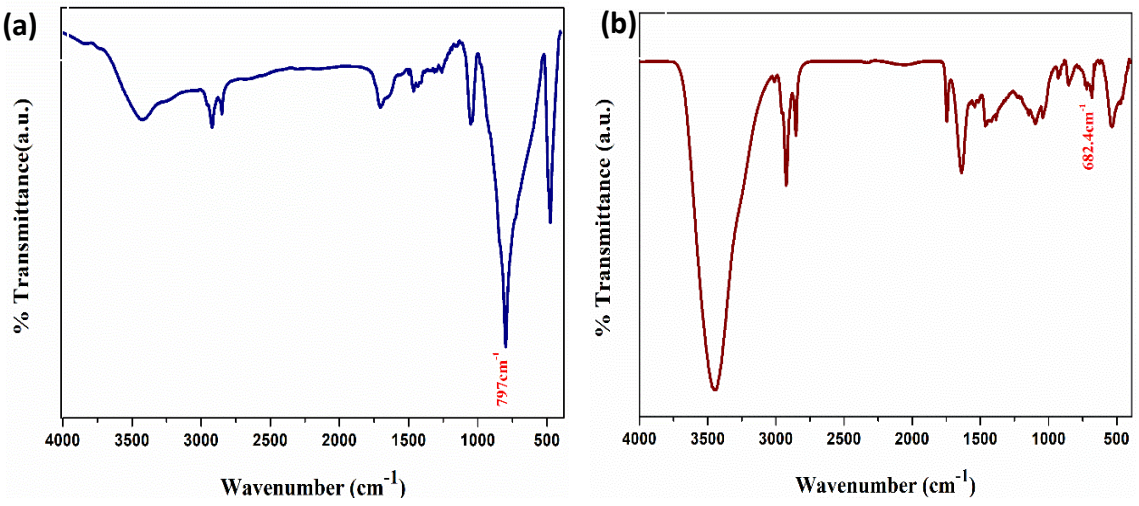

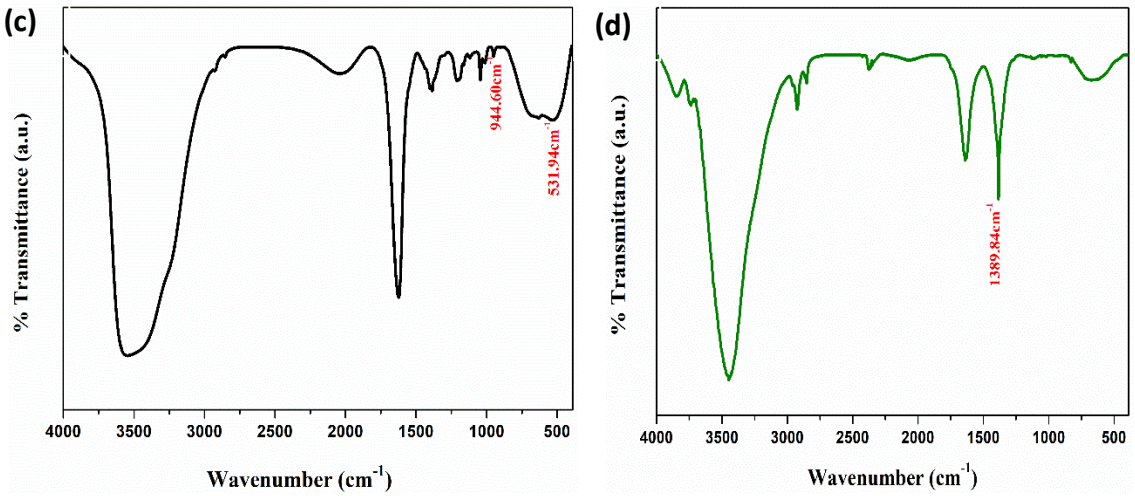

Figure 3.22 FT-IR spectra after adsorption of metal ions (a)Arsenic, (b)Lead, (c)Cadmium, and (d)Chromium from aqueous surface

From the data attained through SEM, SEM-EDX, and FT-IR after the adsorption of ionic species, it can be apprehended that the active sites of the gel got incorporated with the adsorbed species and the presence of the same can be perceived from EDX spectra.

3.8.3 Adsorption of metal ions

The metal adsorption capacity of the organogel increases rapidly with the increase in the time of adsorption by the sorbent. The adsorbent can reduce the concentration of certain heavy metals ranging from 954 ppm to 194ppm for As^{3+} ion, 27.8 ppm to 8.2ppm for Pb^{2+}, 7.85 ppm to 3.08ppm for Cd^{2+}, 190.66ppm to 55.82ppm for Cr^{3+} with a removal efficiency of 79.68%, 70.50%, 60.76%, and 70.72% (Table 3.8 and Figure 3.24). This efficiency rate for the removal of ionic species can be speculated due to the presence of negatively charged sulfonic groups acting as an active site for the adsorption of ionic species interconnecting electrostatically. The adsorption capacity (Qe) and percent removal were determined using equations (i) and (ii). The adsorption capacity was seen to be highest in Arsenic with 570.42mg/g, about 101.13mg/g in Chromium, 14.7mg/g for Lead, and 3.5mg/g in Cadmium. A competent list of adsorbents with their highest adsorption capacity the for removal of arsenic has been prepared in Table 3.11.

It was observed that within the first hour of evaluation, the sorbent was able to adsorb around 72.97% of As(III), 48.56% of Pb(II), 55.54% of Cd(II), and 57.59% of Cr(III) (Figure 3.23) from the aqueous solution which is due to the probable active

available sites in the sorbent capable of adsorbing metals ions due to the presence of strong electrostatic attraction.

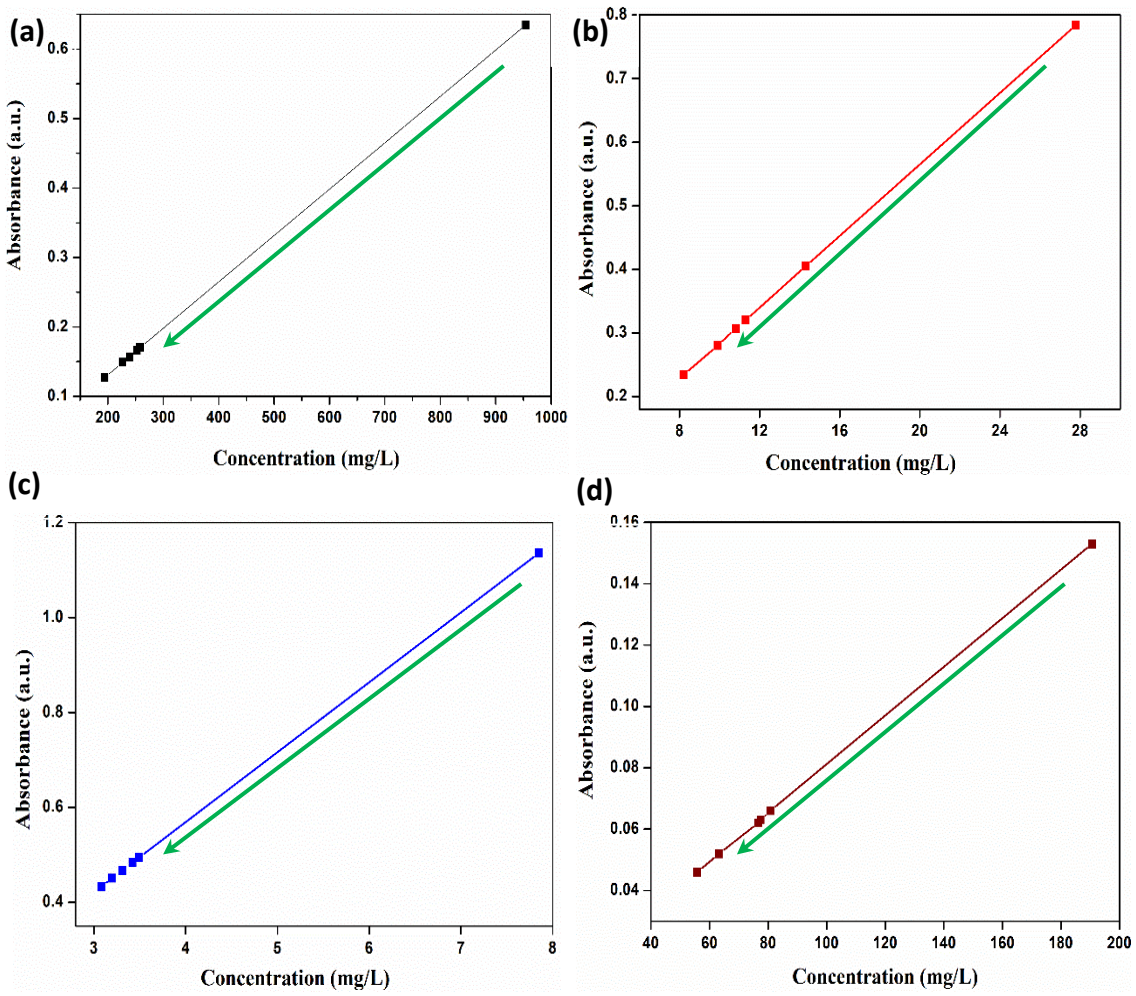

Figure 3.23 AAS data obtained after adsorption of (a)Arsenic, (b)Lead, (c)Cadmium, and (d)Chromium ions with usage of organogel

Table 3.8 Adsorption percentage with values of initial and final concentration of metal ions

Sl No.	Metals used	Weight of adsorbent (g)	Initial concentration (ppm)	Final Concentration (ppm)	Amount adsorbed (mg/g)	Adsorption Percentage (%)
1.	As	0.3	954	194	570.42	**79.68**
2.	Pb	0.3	27.8	8.2	14.7	**70.50**
3.	Cd	0.3	7.85	3.08	3.5	**60.76**
4.	Cr	0.3	190.66	55.82	101.13	**70.72**

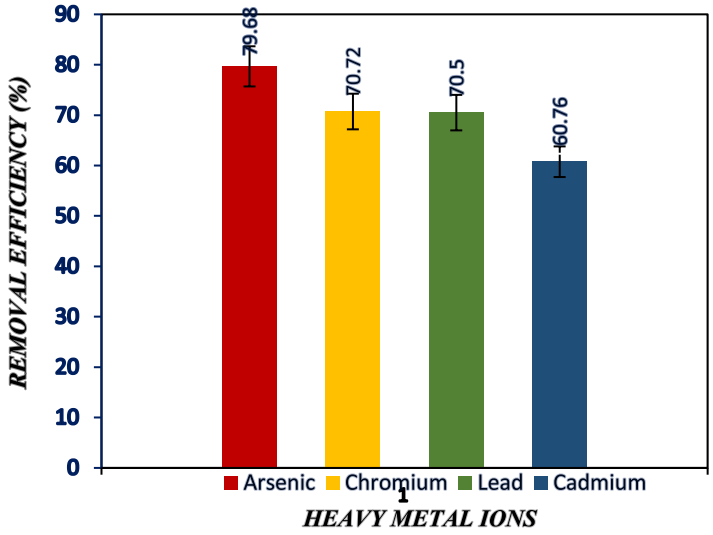

Figure 3.24 Removal percentage (Re%) of the metal ions by the organogel

The absorbing capacity was seen to be the highest for extremely toxic Arsenite (570.42 mg/g) with the highest concentration of around 1000ppm making it the most suitable metal for the fastest removal from groundwater. The observed phenomenon can be attributed to the inherent chemical properties of arsenic as a hard acid. Its strong interaction with the hard base present in the active sites of the gel facilitates the formation of acid-base entities. This strong thermodynamic affinity enables the establishment of potent acid-base complexes, while the kinetic aspect allows arsenic to react more quickly with the hard base. The removal percentage of the metal ions would broadly imply the further removal of heavy metallic pollutants as contaminants from water resources. The aspect of the current work can also be applied to the removal of transition metal pollutants from wastewater sources.

3.8.4 XPS analysis

The removal efficiency of arsenic was found to be higher compared to cadmium, chromium, and lead. XPS analysis helped to validate the adsorption of arsenic by the organogel and confirm the chemical compositions on the surface of the gel. High-resolution XPS spectra of arsenic-adsorbed gel can be observed in Figure 3.25a. In addition to the previously present elements in gel i.e., carbon, nitrogen, oxygen, and sulphur, the adsorbed metal arsenic was also found to be present. Resolutions of C1s, O1s, N1s, S2p with As3d were also analyzed as observed in Figure 3.25 (b,c,d,e,f).

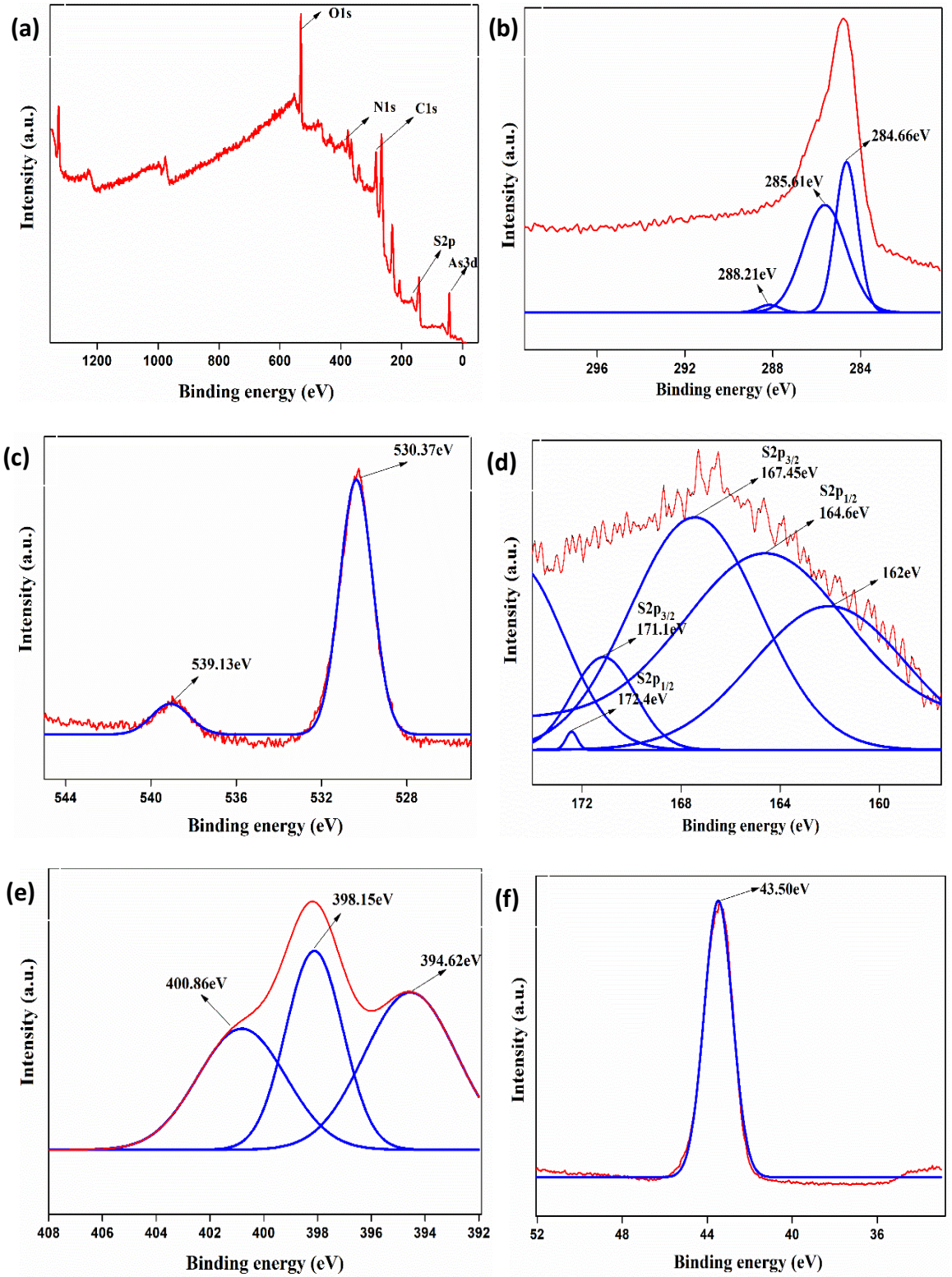

Figure 3.25 (a)XPS spectra of the metal adsorbed organogel, Curve fitting of (b)C1s, (c)O1s, (d)S2p, (e)N1s, (f)As3d spectra

Deconvolution of the C1s peak into three peaks with binding energies 284.66 eV, 285.61 eV, and 288.21 eV contributes to the C–C, C–O–C, and O–C=O respectively [19]. The spectra for O1s observed at 530.37 eV and 539.13 eV correspond to the C–O,

C=O and HO–C [19]. The S2p spectra were further deconvoluted to five peaks with 162 eV, 164.6 eV, 167.4 eV, 171.1 eV, and 172.4 eV as the binding energies. 167.4 eV was due to the SO_3^- sulphite group and 162 eV to the S–O–As interaction [30]. The overlapping of spin-orbit doublets can be seen in S2p due to which the $Sp_{3/2}$ and $Sp_{1/2}$ peaks [31] resulted in a 2:1 ratio. While binding energies at 394.62 eV, 398.15 eV, and 400.86 eV of N1s attributes to C–NH, C–N–C, N–(C=O) [32]. The binding energy of arsenic being observed at 43.50 eV experienced a slight shifting from its original binding energy of 44.7 eV [33]. This confirms the interaction of the metal with the organogel on its active surface. Similar conclusions can thus be drawn for the other heavy metals.

3.8.5 Study of pH

A change in the pH of a solution affects the efficiency of metal adsorption. An aqueous solution of the metal (As, Pb, Cd) with pH value (4,7,9) was prepared while calibrating with 0.1M HCl and 0.1M NaOH. The removal efficiency of the gel increased with an increase in pH from 4 to 7 while rapidly decreasing with a further increase of pH from 7 to 9. The removal percentage for As, Pb, and Cd was found to be the highest with 76.29%, 71.28%, and 59.86% at pH 7. As the pH increases beyond 7, there occurs the formation of metal hydroxide reducing interaction between sulfonic groups, hence the adsorption decreases. At pH 4, protonation occurs while slightly lowers adsorption than the neutral pH. Thus, at pH7 being a deprotonated state, removal was seen to be highest. The effect of pH on the removal of metals is shown in Figure 3.26a.

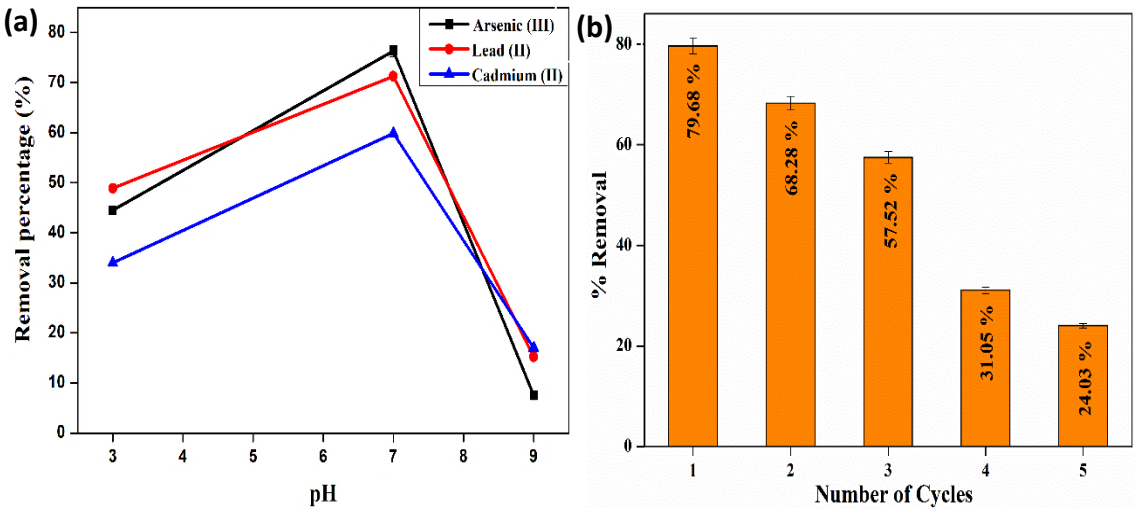

Figure 3.26 (a) Effect of pH on removal of metal ions, (b) Recyclability study of the As(III) metal by the sorbent

The recyclability study by the adsorbent/organogel has been performed with Arsenic ion (Figure 3.26b). The sorbent was used to observe the recycle factor by using it for 5times. It can be perceived that the sorbent was able to remove 79.68, 68.28, 57.52, 31.05, and 24.03 percent of the arsenic metal in its respective 5 cycles. However, it can be used effectively only for three repetitive cycles with removal up to 57% in 3rd cycle as significant decrease was observed in 4th and 5th cycle with 31% and 24%.

3.8.6 Kinetics of adsorption

The time-dependent adsorption efficacies between sorbent and metal ions were studied using first and second-order kinetic models from equations (iii) and (v) from section 2.2.5 of Chapter 2.

$$ln(q_e - q_t) = lnq_e - k_1 t$$

and

$$t/q_t = t/q_e + 1/k_2 q_e^2$$

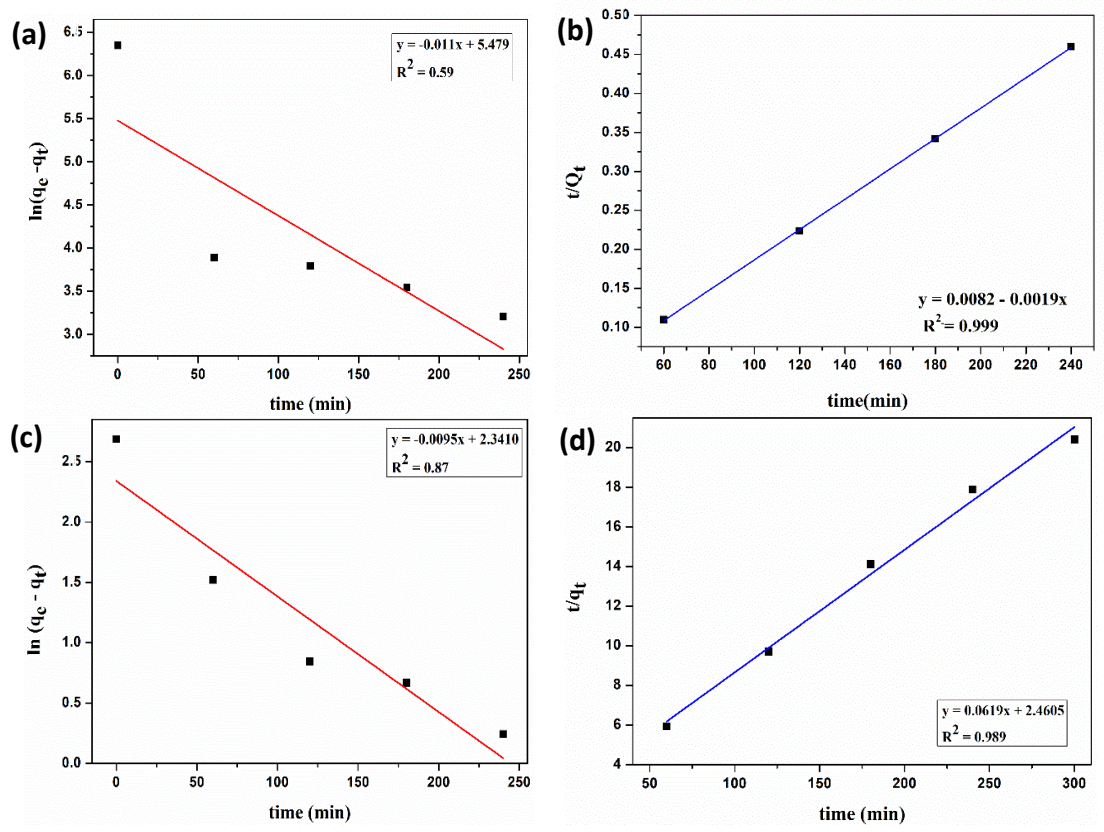

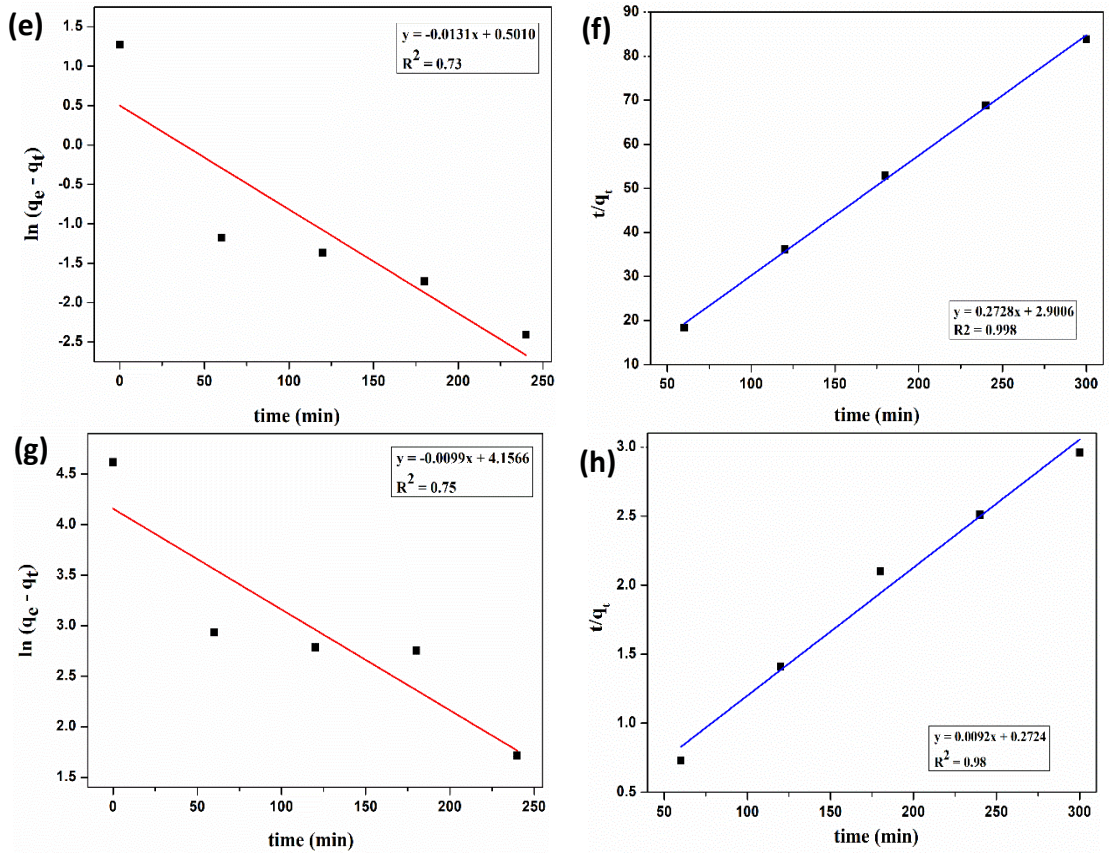

Figure 3.27 The plot of ln(qe-qt) vs time for (a,c,e,g) and plot of t/qt vs time (b,d,f,h) graph for adsorbed metal Arsenic, Lead, Cadmium, Chromium

From the above obtained fitted curves in Figure 3.27 for pseudo first and second order kinetic models, it has been observed that the curves provide a higher correlation with that of second order kinetics model due to the value of regression coefficient, R^2 closer to 1(0.98-0.99) indicating the adsorption of ionic species by the active sites of the sorbent. Values of k_1 and k_2 with respective correlation coefficients can be acquired from Table 3.10.

3.8.7 Adsorption Isotherm

Isothermal adsorption was studied to determine the behaviour of sorbent for metal removal using Langmuir, Freundlich, and Temkin isotherms from equations (iv), (v), and (vi) from Section 3.3.3.3 respectively.

$$C_e/q_e = C_e/q_{max} + 1/K_L \times q_{max}$$

$$lnq_e = lnK_F + (1/n)\, lnC_e$$

$$q_e = BlnK_T + BlnC_e$$

The parametric values for different isotherms can be obtained from Table 3.9.

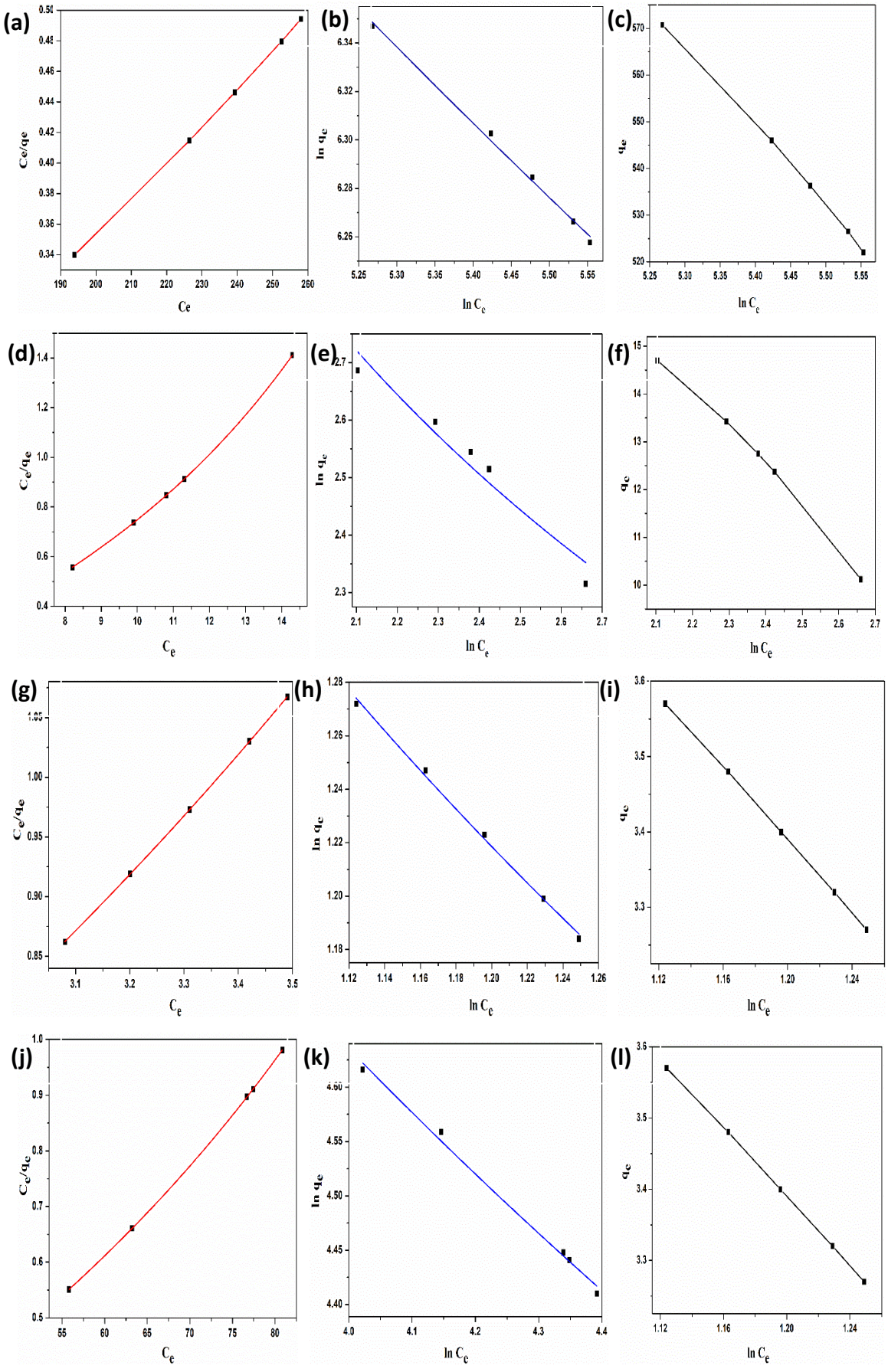
(a)
Ce/qe
Ce
(b)
ln qe
ln Ce
(c)
qe
ln Ce
(d)
Ce/qe
Ce
(e)
ln qe
ln Ce
(f)
qe
ln Ce
(g)
Ce/qe
Ce
(h)
ln qe
ln Ce
(i)
qe
ln Ce
(j)
Ce/qe
Ce
(k)
ln qe
ln Ce
(l)
qe
ln Ce

Figure 3.28 Adsorption isotherm of plot Ce/qe vs Ce (a,d,g,j), lnqe vs lnCe (b,e,h,k), qe vs ln Ce (c,f, i,l) for adsorbed metal ions Arsenic (III), Lead (II), Cadmium (II), Chromium (III)

Table 3.9 Isothermic parameters for metal removal obtained from plotted curves

ISOTHERMS	PARAMETERS	As (III)	Pb (II)	Cd (II)	Cr (III)
LANGMUIR	K_L (L/mg)	0.001	0.036	0.286	2.352
	R^2	**1**	**1**	**0.999**	**1**
	R_L	0.511	0.49	0.30	0.002
FREUNDLICH	1/n	0.26	1.62	1.46	1.93
	$K_F(mg^{(1-1/n)}/L^{1/n}.g^{-1})$	0.987	1.116	1.379	2.671
	R^2	0.994	0.93	0.995	0.991
TEMKIN	$A(L.g^{-1})$	4.74E41	1.12E42	1.81E42	4.84E26
	B	5.53	0.129	0.034	1.429
	$b_T(kJ\ mol^{-1})$	0.448	19.205	72.869	1.733
	R^2	0.40	0.41	0.36	0.35

A close-fitting was observed from all three isothermal models (Figure 3.28). Higher correlation can be attained from the above-fitted curves for Langmuir isotherm [35,36] with a regression value of 1 representing that adsorption of metal ions proceeds through monolayer deposition over the external sorbent surface along with the strong electrostatic force of attraction observed metal ions and active positions of the sorbent. A lower 1/n value from the Freundlich isotherm also signifies that monolayer deposition occurred through a chemical process. Higher value of 1/n represents that the interaction between adsorbate and adsorbent is conveniently low contradicting the theory of multilayer deposition [37]. Since $0 < 1/n < 1$, the results of arsenic compiled both types of adsorption chemisorption along physisorption. According to the regression values of both isotherms, Langmuir isotherm observed an R^2 value of 1 in contrast to 0.994 of Freundlich isotherm. Hence arsenic observed Langmuir monolayer adsorption followed by multilayer deposition. This may be one of the prime reasons for the increase in removal percentage among all the heavy metals used. Contracting to the finding of isotherm for arsenic, the 1/n value for the rest of the heavy metals lies beyond 1, which does not fall into the criterion of multilayer deposition, thus following Langmuir's adsorption isotherm of monolayer deposition. The R_L values 0.51, 0.49, 0.30, 0.002 of metals arsenic, lead, cadmium and chromium lie in between and 1 where $0 < R_L < 1$ is

considered favorable, R_L=1 is linear while R_L > 1 is unfavorable and R_L= 0 is irreversible. This indicates the favorability of metal adsorption by the gels [38].

3.8.8 Model of mass transfer

The fitted curve of qt against $t^{1/2}$ from the Weber-Morris model (equation vii of section 3.3.3.4) of diffusion (intra-particle) for adsorption of $As^{(3+)}$, $Pb^{(2+)}$. $Cd^{(2+)}$, and $Cr^{(3+)}$ denote a multi-stage adsorption process obtained from Figure 3.29.

$$q_t = k_{id}t^{1/2} + c$$

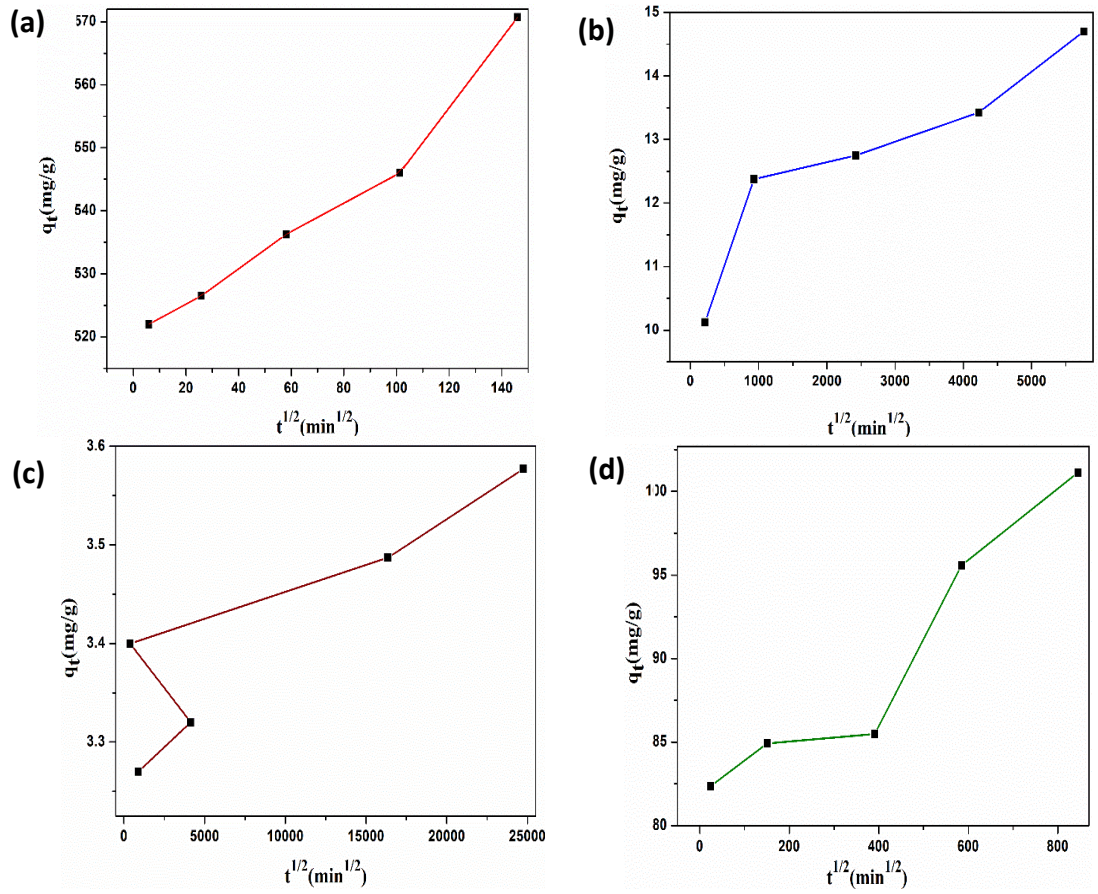

Figure 3.29 Intra-particle diffusion plot of q_t vs $t^{1/2}$ after metal adsorption

For all the metal ionic species, the curve demonstrated multi-stage adsorption processes. The values for diffusion parameters can be attained from Table 3.10. Since the curve of q_t vs $t^{1/2}$ plot (Figure 3.29) does not pass through the center of origin, it signifies that the adsorption is controlled by more than one kinetic step. The first step includes the infusion of the metal ions from the solution to the surface of the sorbent. The second step involves the interaction of the metal ions with active sites of the surface followed by the third step where adsorption continues until all the active sites have been covered

attaining equilibrium position. C (intercept) representing the boundary layer thickness (mg/g) indicates the influence of surface adsorption in rate limiting step. An increase in the intercept value indicates increase in adsorption on the surface [45]. Among the four metals Arsenic (III) was found to adsorb around 517.75mg/g, Lead (II) about 10.85mg/g, Cadmium (II) by 3.31mg/g and Chromium (III) with 80.57mg/g. Adsorption amount obtained from the diffusion model correlates with the adsorption capacity (q_e) value from Table 3.8 thus confirming the adsorption value.

Table 3.10 Kinetics parameters for removal of metal ions

SAMPLE	pseudo-first-order model		pseudo-second-order model		Intra-particle diffusion model		
	$k_1(min^{-1})$	R^2	$k_2(gg^{-1}min^{-1})$	R^2	k_{id}	C	R^2
As (III)	4.913×10^{-4}	**0.59**	0.122×10^{-4}	**0.99**	0.229×10^{-2}	517.75	**0.96**
Pb(II)	0.116×10^{-4}	**0.87**	0.118×10^{-4}	**0.98**	0.116×10^{-6}	10.85	**0.79**
Cd(II)	0.022×10^{-4}	**0.73**	0.113×10^{-4}	**0.99**	0.421×10^{-9}	3.31	**0.76**
Cr(III)	0.923×10^{-4}	**0.75**	0.117×10^{-4}	**0.98**	0.276×10^{-4}	80.57	**0.88**

3.8.9 Mechanism of adsorption

The mechanism of metal adsorption can be explicated owing to the presence of sulfonate anion SO_3^- of acrylamidomethylpropane sulfonic acid which binds with the metal ion present by bridging linkages [46,47] as bidentate and tetradentate ligand for M^{2+} and M^{3+} ions respectively eventually alleviating the capture of heavy metal ions from groundwater (Figure 3.30). Similar concomitance can be drawn from the mechanism while carrying out the adsorption process on three transition metals as well viz. Nickel, Copper, and Cobalt ions with adsorption capacity values of 2.30mg/g, 1.46mg/g, and 1.26mg/g correspondingly. The presence of the same can be detected using electron microscopic images (Figure 3.31) along with substantiation by EDX analysis, thus proving the adsorbent to be economical and effective for the removal of heavy metals alongside transition metals for sustainability purposes.

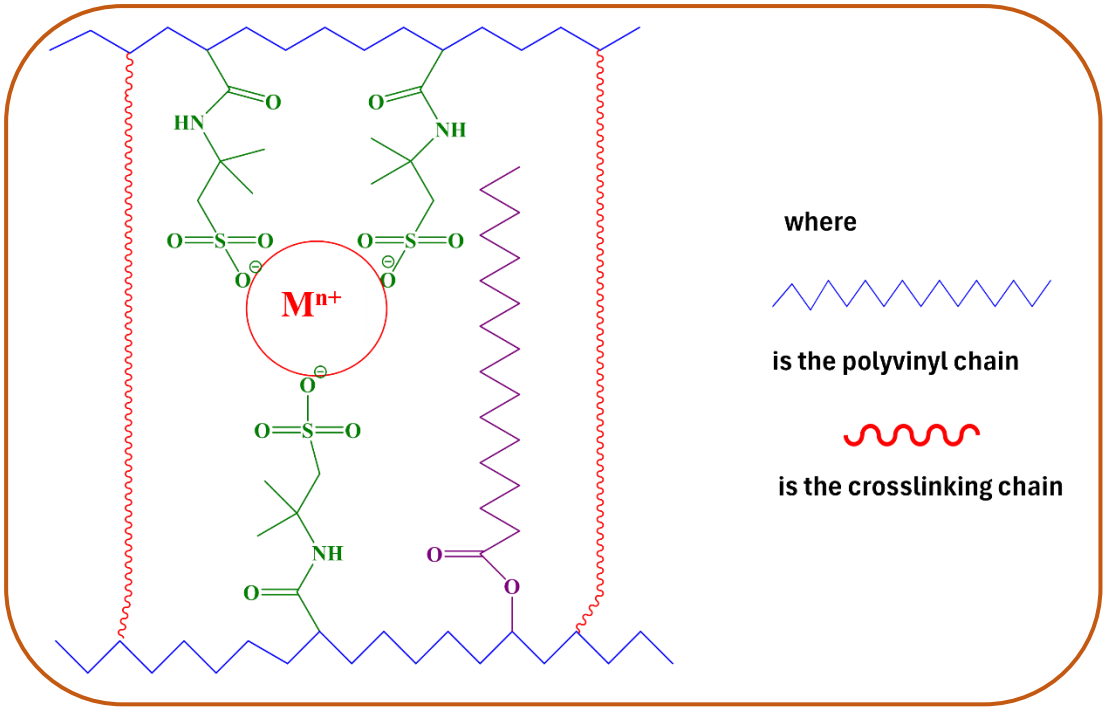

Figure 3.30 Mechanistic representation of the bridging linkage to capture metal ions

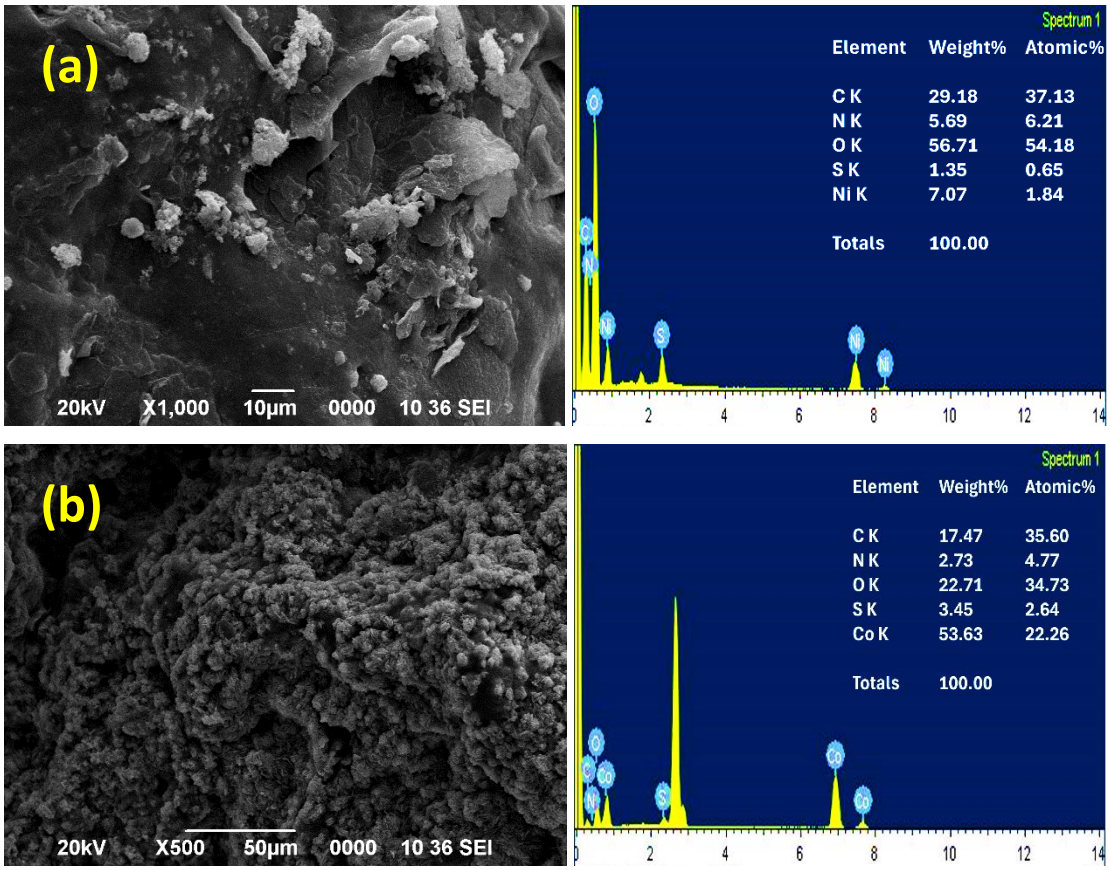

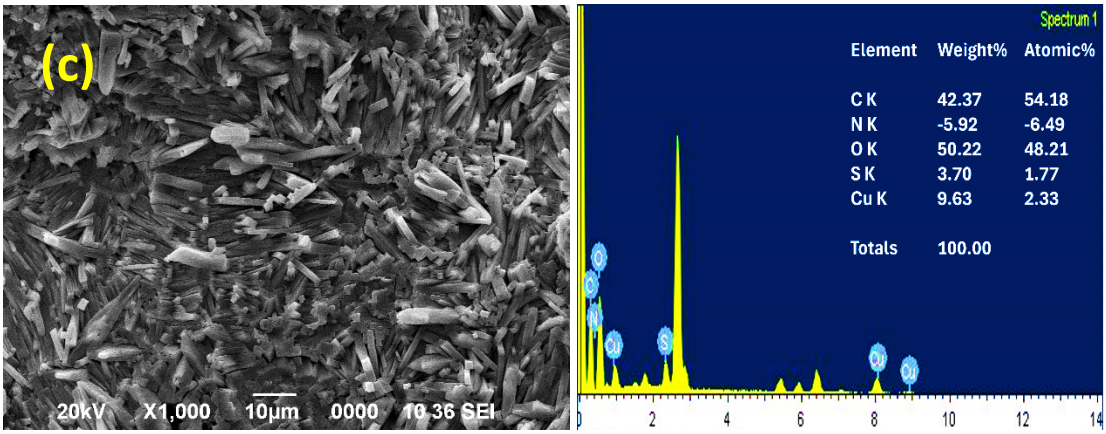

Figure 3.31 Morphological images and SEM-EDX analysis of metal ions after adsorption (a)Nickel, (b)Cobalt, (c)Copper from surface water

Table 3.11 Comparable chart of the organogel for Arsenic removal with other sorbents

ADSORBENT	ARSENIC SPECIES	ADSORPTION CAPACITY (mg/g)	REFERENCE
Magnetic Wheat Straw	(III)	30.24	[48]
Stable maghemite (γ -Fe_2O_3) loaded pumice	(III)	30.36	[49]
Goethite modified biochar	(III)	65.3	[50]
Granular ferric hydroxide	(III)	66	[51]
α-FeOOH modified biochar (single adsorption)	(III)	78.3	[52]
Coprecipitated bimetal oxide magnetic Nanomaterials: (i) $MnFe_2O_4$	(III)	94	[53]
(ii) $CoFe_2O_4$	(III)	100	
Biogenic Schwertmannite	(III)	113.9	[54]
Hydrous cerium oxide nanoparticles	(III)	170	[55]
Synthetic Iron Oxides: (i) Akaganeite	(III)	148.7	[56]
(ii) Modified Akaganeite	(III)	200	
Polymeric Organogel	(III)	570.42	This Work
Immobilized plant biomass-Garcinia cambogia	(III)	704.11	[57]

3.9 CONCLUSION

This study focuses exclusively on the removal of metallic waste deposited in water resources, which poses a threat to human health and aquatic organisms. A

polymeric sorbent has been developed using a cost-effective and simple method to effectively eliminate heavy metal ions, such as arsenic, lead, cadmium, and chromium, commonly found in groundwater. The sorbent demonstrated a successful removal rate of approximately 79.68% for arsenic, 70.50% for lead, 60.76% for cadmium, and 70.72% for chromium from wastewater, presenting a promising approach for heavy metal removal through sorption. Additionally, experiments conducted with transition metal ions (nickel, cobalt, and copper) yielded similar results to those obtained with heavy metals.

The sorbent adheres to the kinetic mechanism of the pseudo-second-order model and follows the Langmuir adsorption isotherm, which involves the deposition of a monolayer of particles through the chemisorption process. The time-dependent intra-particle diffusion model revealed that the rate-determining step and second-order rate kinetics are involved in the process. The primary mechanism entails electrostatic interactions between the adsorbent and adsorbate molecules of varying sizes, making it a promising and sustainable sorbent for the removal of metallic pollutants from contaminated water sources.

3.10 REFERENCES

[1] Qasem, N. A. A., Mohammed, R. H., and Lawal, D. U. Removal of Heavy Metal Ions from Wastewater: A Comprehensive and Critical Review. *NPJ Clean Water*, 4 (36), 2021.

[2] Al-Senani, G. M., and Al-Fawzan, F. F. Adsorption Study of Heavy Metal Ions from Aqueous Solution by Nanoparticle of Wild Herbs. *Egyptian Journal of Aquatic Research*, 44 (3), 187–194, 2018.

[3] Liu, Y., Pang, H., Wang, X., Yu, S., Chen, Z., Zhang, P., Chen, L., Song, G., Saleh Alharbi, N., Omar Rabah, S., and Wang, X. Zeolitic Imidazolate Framework-Based Nanomaterials for the Capture of Heavy Metal Ions and Radionuclides: A Review. *Chemical Engineering Journal*, 406, 127139, 2021.

[4] Olawale, S. A., Bonilla-Petriciolet, A., Mendoza-Castillo, D. I., Okafor, C. C., Sellaoui, L., and Badawi, M. Thermodynamics and Mechanism of the Adsorption of Heavy Metal Ions on Keratin Biomasses for Wastewater Detoxification. *Adsorption Science and Technology*, 2022, 7384924, 2022.

[5] Gupta, S. K., and Chen, K. Y. Arsenic Removal by Adsorption. *Journal of the Water Pollution Control Federation*, 50: 493-506, 1978.

[6] Wani, A. L., Ara, A., and Usmani, J. A. Lead Toxicity: A Review. *Interdisciplinary Toxicology*, 8: 55–64, 2015.

[7] Shekhawat, K., Chatterjee, S., and Joshi, B. Chromium Toxicity and its Health Hazards. *International Journal of Advanced Research*, 3 (7): 167-172, 2015.

[8] Kong, W., Yue, Q., Li, Q., and Gao, B. Adsorption of Cd 2+ on GO/PAA Hydrogel and Preliminary Recycle to GO/PAA-CdS as Efficient Photocatalyst. *Science of the Total Environment*, 668: 1165–1174, 2019.

[9] Marchetti, P., Solomon, M. F. J., Szekely, G., and Livingston, A. G. Molecular Separation with Organic Solvent Nanofiltration: A Critical Review. *Chemical Reviews*, 114 (21): 10735–10806, 2014.

[10] Isosaari, P., and Sillanpää, M. Effects of Oxalate and Phosphate on Electrokinetic Removal of Arsenic from Mine Tailings. *Separation and Purification Technology*, 86: 26–34, 2012.

[11] Tong, S., Shen, J., Jiang, X., Li, J., Sun, X., Xu, Z., and Chen, D. Recycle of Fenton Sludge through One-Step Synthesis of Aminated Magnetic Hydrochar for Pb2+ Removal from Wastewater. *Journal of Hazardous Materials*, 406, 124581, 2021.

[12] Wei, Y., Cheng, X., Ding, A., and Xu, J. Magnesium Silicate Polymer as a Coagulant for Reactive Dye Removal from Wastewater: Considering the Intrinsic PH in Magnesium Silicate Polymer and Coagulation Behavior. *ACS Omega*, 5 (40), 26094–26100, 2020.

[13] Li, W.; Zhang, Y.; Liu, T.; Huang, J.; Wang, Y. Comparison of Ion Exchange and Solvent Extraction in Recovering Vanadium from Sulfuric Acid Leach Solutions of Stone Coal. *Hydrometallurgy*, 131–132: 1–7, 2013.

[14] Chakraborty, R., Asthana, A., Singh, A. K., Jain, B., and Susan, A. B. H. Adsorption of Heavy Metal Ions by Various Low-Cost Adsorbents: A Review. *International Journal of Environmental Analytical Chemistry*, 102 (2): 342–379, 2022.

[15] Gautam, R. K., Mudhoo, A., Lofrano, G., and Chattopadhyaya, M. C. Biomass-Derived Biosorbents for Metal Ions Sequestration: Adsorbent Modification and

Activation Methods and Adsorbent Regeneration. *Journal of Environmental Chemical Engineering*, 2 (1): 239–259, 2014.

[16] Meena, A. K., Mishra, G. K., Rai, P. K., Rajagopal, C., and Nagar, P. N. Removal of Heavy Metal Ions from Aqueous Solutions Using Carbon Aerogel as an Adsorbent. *Journal of Hazardous Materials*, 122 (1–2): 161–170, 2005.

[17] Afroze, S., and Sen, T. K. A Review on Heavy Metal Ions and Dye Adsorption from Water by Agricultural Solid Waste Adsorbents. *Water, Air, & Soil Pollution*, 229, 225, 2018.

[18] Kian, L. K., Jawaid, M., Mahmoud, M. H., Saba, N., Fouad, H., Alothman, O. Y., and Karim, Z. PBAT/PBS Blends Membranes Filled with Nanocrystalline Cellulose for Heavy Metal Ion Separation. *Journal of Polymers and the Environment*, 30 (12): 5263–5273, 2022.

[19] Chen, J., Jiang, X., Yin, D., and Zhang, W. Preparation of a Hydrogel-Based Adsorbent for Metal Ions through High Internal Phase Emulsion Polymerization. *ACS Omega*, 5 (32): 19920–19927, 2020.

[20] Tran, T. H., Okabe, H., Hidaka, Y., and Hara, K. Removal of Metal Ions from Aqueous Solutions Using Carboxymethyl Cellulose/Sodium Styrene Sulfonate Gels Prepared by Radiation Grafting. *Carbohydrate Polymers*, 157: 335–343, 2017.

[21] Godiya, C. B., Cheng, X., Li, D., Chen, Z., and Lu, X. Carboxymethyl Cellulose/Polyacrylamide Composite Hydrogel for Cascaded Treatment/Reuse of Heavy Metal Ions in Wastewater. *Journal of Hazardous Materials*, 364: 28–38, 2019.

[22] M'hamed, M. O., and Khezami, L. 1,2,3,4-Tetrahydropyrimidine Derivative for Selective and Fast Uptake of Cadmium Ions from Aqueous Solution. *Environments*, 6 (6): 68, 2019.

[23] Liao, J., Liu, P., Xie, Y., and Zhang, Y. Metal Oxide Aerogels: Preparation and Application for the Uranium Removal from Aqueous Solution. *Science of the Total Environments*, 768, 144212, 2020.

[24] Kobielska, P. A., Howarth, A. J., Farha, O. K., and Nayak, S. Metal–Organic Frameworks for Heavy Metal Removal from Water. *Coordination Chemistry Reviews*, 358: 92–107, 2018.

[25] Chu, L., Liu, C., Zhou, G., Xu, R., Tang, Y., Zeng, Z., and Luo, S. A Double Network Gel as Low Cost and Easy Recycle Adsorbent: Highly Efficient Removal of Cd(II) and Pb(II) Pollutants from Wastewater. *Journal of Hazardous Materials*, 300: 153–160, 2015.

[26] Ma, J., Luo, J., Liu, Y., Wei, Y., Cai, T., Yu, X., Liu, H., Liu, C., and Crittenden, J. C. Pb(II), Cu(II) and Cd(II) Removal Using a Humic Substance-Based Double Network Hydrogel in Individual and Multicomponent Systems. *Journal of Materials Chemistry A*, 6 (41): 20110–20120, 2018.

[27] Charerntanyarak, L. Heavy Metals Removal by Chemical Coagulation and Precipitation. *Water Science and Technology*, 39 (10-11): 135–138, 1999.

[28] Zhou, G., Luo, J., Liu, C., Chu, L., and Crittenden, J. Efficient Heavy Metal Removal from Industrial Melting Effluent Using Fixed-Bed Process Based on Porous Hydrogel Adsorbents. *Water Research*, 131: 246–254, 2018.

[29] Baruah, K., Dutta, R., Doley, S., and Dolui, S. K. Grafted Polymeric Organogel Using Low Molecular Weight Gelator as an Effective Medium for Expulsion and Purification of Cationic Dyes and Organic Pollutants from Contaminated Surface Water. *European Polymer Journal*, 195, 112213, 2023.

[30] Castner, D. G., Hinds, K., and Grainger, D. W. X-Ray Photoelectron Spectroscopy Sulfur 2p Study of Organic Thiol and Disulfide Binding Interactions with Gold Surfaces. *Langmuir*, 12 (21): 5083-5086, 1996.

[31] Syed, J. A., Sardar, S. A., Yagi, S., and Tanaka, K. Sulfur Edge XANES and XPS Spectroscopy of Ethanethiol Adsorbed on Nickel. *Surface Science*, 566–568 (1): 597–602, 2004.

[32] Wu, J., Wang, W., and Wang, Z. Porphin-Based Carbon Dots for “Turn off–on” Phosphate Sensing and Cell Imaging. *Nanomaterials*, 10 (2), 326, 2020.

[33] Yang, K., Qin, W., and Liu, W. Extraction of Metal Arsenic from Waste Sodium Arsenate by Roasting with Charcoal Powder. *Metals*, 8 (7), 542, 2018.

[34] Guidelines for drinking-water quality: fourth edition incorporating the first addendum. Geneva: World Health Organization. ISBN: 9789241549950, 2017.

[35] Dutta, S., Srivastava, S. K., Gupta, B., and Gupta, A. K. Hollow Polyaniline Microsphere/MnO2/Fe3O4nanocomposites in Adsorptive Removal of Toxic Dyes from Contaminated Water. *ACS Applied Materials Interfaces*, 13 (45), 54324–54338, 2021.

[36] Kalam, S., Abu-Khamsin, S. A., Kamal, M. S., and Patil, S. Surfactant Adsorption Isotherms: A Review. *ACS Omega*, 6 (48): 32342–32348, 2021.

[37] Shikuku, V. O., and Mishra, T. Adsorption Isotherm Modeling for Methylene Blue Removal onto Magnetic Kaolinite Clay: A Comparison of Two-Parameter Isotherms. *Applied Water Science*, 11 (6), 103, 2021.

[38] Yang, X., Li, Y., Du, Q., Sun, J., Chen, L., Hu, S., Wang, Z., Xia, Y., and Xia, L. Highly Effective Removal of Basic Fuchsin from Aqueous Solutions by Anionic Polyacrylamide/Graphene Oxide Aerogels. *Journal of Colloid and Interface Science*, 453 (122): 107–114, 2015.

[39] Alharbi, R. M., Sholkamy, E. N., Alsamhary, K. I., Abdel-Raouf, N., and Ibraheem, I. B. M. Optimization Study of the Capacity of Chlorella Vulgaris as a Potential Bio-Remediator for the Bio-Adsorption of Arsenic (III) from Aquatic Environments. *Toxics*, 11 (5), 439, 2023.

[40] Mandal, S., Sahu, M. K., and Patel, R. K. Adsorption Studies of Arsenic(III) Removal from Water by Zirconium Polyacrylamide Hybrid Material (ZrPACM-43). *Water Resources and Industry*, 4: 51–67, 2013.

[41] Raza, J., Hamid, A., Khan, M., Hussain, F., Tiehu, L., Fazil, P., Zada, A., Wahab, Z., and Ali, A. Spectroscopic Characterization of Biosynthesized Lead Oxide (PbO) Nanoparticles and Their Applications in PVC/Graphite-PbO Nanocomposites. *Zeitschrift fur Physikalische Chemie*, 236 (5): 619–636, 2022.

[42] Lefojane, R. P., Sone, B. T., Matinise, N., Saleh, K., Direko, P., Mfengwana, P., Mashele, S., Maaza, M., and Sekhoacha, M. P. CdO/CdCO3 Nanocomposite Physical Properties and Cytotoxicity against Selected Breast Cancer Cell Lines. *Scientific Reports*, 11, 30, 2021.

[43] Nallendran, R., Selvan, G., and Balu, A. R. CdO-Fe3O4 Nanocomposite with Enhanced Magnetic and Photocatalytic Properties. *Materials Science*- Poland, 37 (1), 100–107, 2019.

[44] Guo, Y., Zhao, N., Zhang, T., Gong, H., Ma, H., An, T., Zhao, F., and Hu, R. Compatibility and Thermal Decomposition Mechanism of Nitrocellulose/Cr 2 O 3 Nanoparticles Studied Using DSC and TG-FTIR. *RSC Advances*, 9 (7): 3927–3937, 2019.

[45] Pholosi, A., Naidoo, E. B., and Ofomaja, A. E. Intraparticle Diffusion of Cr (VI) through Biomass and Magnetite Coated Biomass: A Comparative Kinetic and Diffusion Study. *South African Journal of Chemical Engineering*, 32: 39–55, 2020.

[46] Hao, L., Liu, M., Wang, N., and Li, G. A Critical Review on Arsenic Removal from Water Using Iron-Based Adsorbents. *RSC Advances*, 8: 39545–39560, 2018.

[47] Kapoor, R., Wadhawan, P., and Kapoor, P. Preparation, Properties, and Characterization of Methanesulfonato Complexes of Arsenic (III), Antimony (III), and Bismuth (III). *Canadian Journal of Chemistry*, 65 (6), 1987.

[48] Tian, Y., Wu, M., Lin, X., Huang, P., and Huang, Y. Synthesis of Magnetic Wheat Straw for Arsenic Adsorption. *Journal of Hazardous Materials*, 193: 10–16, 2011.

[49] Ranjan, S., Yadav, B. K., and Joshi, H. Removal of Arsenic (III and V) from Aqueous Solution Using Stable Maghemite (γ -Fe2 O3) Loaded Pumice Composite. *International Journal of Environmental Science and Technology*, 19 (6): 4737–4748, 2022.

[50] Zhu, S., Zhao, J., Zhao, N., Yang, X., Chen, C., and Shang, J. Goethite Modified Biochar as a Multifunctional Amendment for Cationic Cd (II), Anionic As (III), Roxarsone, and Phosphorus in Soil and Water. *Journal of Cleaner Production*, 247, 119579, 2020.

[51] Thirunavukkarasu, O. S., Viraraghavan, T., and Subramanian, K. S. Arsenic Removal from Drinking Water Using Granular Ferric Hydroxide. *Water SA*, 29 (2): 161-170, 2003.

[52] Zhu, S., Qu, T., Irshad, M. K., and Shang, J. Simultaneous Removal of Cd (II) and As (III) from Co-Contaminated Aqueous Solution by α-FeOOH Modified Biochar. *Biochar*, 2 (1): 81–92, 2020.

[53] Zhang, S., Niu, H., Cai, Y., Zhao, X., and Shi, Y. Arsenite and Arsenate Adsorption on Coprecipitated Bimetal Oxide Magnetic Nanomaterials: MnFe2O4 and CoFe2O4. *Chemical Engineering Journal*, 158 (3): 599–607, 2010.

[54] Liao, Y., Liang, J., and Zhou, L. Adsorptive Removal of As (III) by Biogenic Schwertmannite from Simulated As-Contaminated Groundwater. *Chemosphere*, 83 (3): 295–301, 2011.

[55] Li, R., Li, Q., Gao, S., and Shang, J. K. Exceptional Arsenic Adsorption Performance of Hydrous Cerium Oxide Nanoparticles: Part A. Adsorption Capacity and Mechanism. *Chemical Engineering Journal*, 185–186: 127–135, 2012.

[56] Polowczyk, I., Cyganowski, P., Ulatowska, J., Sawiński, W., and Bastrzyk, A. Synthetic Iron Oxides for Adsorptive Removal of Arsenic. *Water, Air, & Soil Pollution*, 229, 203, 2018.

[57] Kamala, C. T., Chu, K. H., Chary, N. S., Pandey, P. K., Ramesh, S. L., Sastry, A. R. K., and Sekhar, K. C. Removal of Arsenic (III) from Aqueous Solutions Using Fresh and Immobilized Plant Biomass. *Water Research*, 39 (13): 2815–2826, 2005.